HAL open science

Petrophysical and magnetic pore network anisotropy of some cretaceous sandstone from Tushka Basin, Egypt

Bassem Nabawy, Pierre Rochette, Yves Géraud

To cite this version:

Bassem Nabawy, Pierre Rochette, Yves Géraud. Petrophysical and magnetic pore network anisotropy of some cretaceous sandstone from Tushka Basin, Egypt. Geophysical Journal International, 2009, 177 (1), pp.43-61. 10.1111/j.1365-246X.2008.04061.x . hal-03698808

HAL Id: hal-03698808

https://hal.univ-lorraine.fr/hal-03698808

Submitted on 26 Jun 2022

HAL is a multi-disciplinary open access archive for the deposit and dissemination of scientific research documents, whether they are published or not. The documents may come from teaching and research institutions in France or abroad, or from public or private research centers.

L'archive ouverte pluridisciplinaire **HAL**, est destinée au dépôt et à la diffusion de documents scientifiques de niveau recherche, publiés ou non, émanant des établissements d'enseignement et de recherche français ou étrangers, des laboratoires publics ou privés.

Distributed under a Creative Commons Attribution 4.0 International License

Geophys. J. Int. (2009) **177,** 43–61 doi: 10.1111/j.1365-246X.2008.04061.x

GJI Geomagnetism, rock magnetism and palaeomagnetism

Petrophysical and magnetic pore network anisotropy of some cretaceous sandstone from Tushka Basin, Egypt

Bassem S. Nabawy,[1] Pierre Rochette[2] and Yves Géraud[3]

[1]*Department of Geophysical Sciences, National Research Center, Cairo, Egypt. E-mail: bsnabawy@yahoo.co.uk*
[2]*Department of Geomagnetism, University of Aix Marseille, France*
[3]*Institut de Physique du Globe de Strasbourg, France*

Accepted 2008 November 27. Received 2008 November 27; in original form 2008 May 20

SUMMARY

Pore magnetic fabric is a well-established technique for the determination of pore elongation and preferred directions for migration of the interstitial fluids. This study further exemplify this technique on a set of the Nubia sandstones through a comparison with the pore anisotropy obtained from measuring permeability in three orthogonal directions in a gaz permeameter. The Nubia sandstones are represented in Tushka area (South Egypt) by quartz arenite of large porosity (29–40 per cent) which was measured on thin sections parallel and perpendicular to the bedding plane and petrophysically by helium pycnometry and ferrofluid injection at 1 bar pressure.

Petrographically, there is a detectable difference between the porosity values in the bedding plane and in the perpendicular direction indicating inhomogeneity in the pore space network distribution.

The petrophysical studies indicate large porosity and permeability values with some differences between the helium and ferrofluid porosity due to presence of micro pore spaces not accessible for the ferrofluid molecules having relatively high diameters and injected at low pressure.

An overall agreement is observed between the permeability anisotropy and the magnetic grain and pore fabrics (magnetic anisotropy measured before and after ferrofluid injection). The three fabrics are mainly dominated by a bedding parallel foliation. In a few cases maximum permeability appears to be perpendicular to bedding. Within the bedding plane, maximum pore elongation direction from ferrofluid injection is NNW for Adindan and Kesieba formations and NW for Abu Simbil Formation. The maximum pore elongation direction for Abu Ballas samples showed a direction fluctuating around the E–W direction, the main fault trends in Tushka area. The pore fabric of Abu Ballas formation seems therefore to be structurally controlled, while it would be originated from palaeocurrent directions in the other formations.

Key words: Magnetic fabrics and anisotrophy; Permeability and porosity.

Downloaded from https://academic.oup.com/gji/article/177/1/43/729241 by guest on 26 June 2022

INTRODUCTION

The main aims of this study are to delineate the permeability and magnetic pore fabrics of the Nubia sequence in Tushka area (south Egypt). The studied area is located between Lat. 22° and 22°45′N and Long. 30°45′ and 31° 45′E (Fig. 1). It is covered mainly by the Nubia sandstones as a type section for these rocks. They extend from south of El-Nuba to the north and could be differentiated into several formations. They have been extensively studied for several decades due to their regional extension and their identification as the most strategic aquifer and reservoir in Egypt. The Nubia sandstones unconformably overly basement rocks and are covered by Quaternary deposits. These sandstone rocks are highly porous with an average bulk porosity of 20 per cent, excluding any secondary porosity introduced by fracturing (Robinson *et al.* 2007). Neither detailed magnetic nor petrophysical studies but some sedimentological and structural studies have been carried out on the Nubia sandstones in south Egypt.

Sedimentary porous rocks could be simulated as two sets of ellipsoids, representing the grain and pore anisotropies. The pore spaces are the main control for the storage capacity of aquifers and reservoir rocks (Nabawy & El-Hariri 2008). Therefore, determination of the elongation of the pore spaces in the 3-D is a main target for the workers in the economic fluids field, for example, in gas, petroleum and groundwater exploration, in particular to detect the preferred direction for economic fluid migration.

© 2009 The Authors
Journal compilation © 2009 RAS

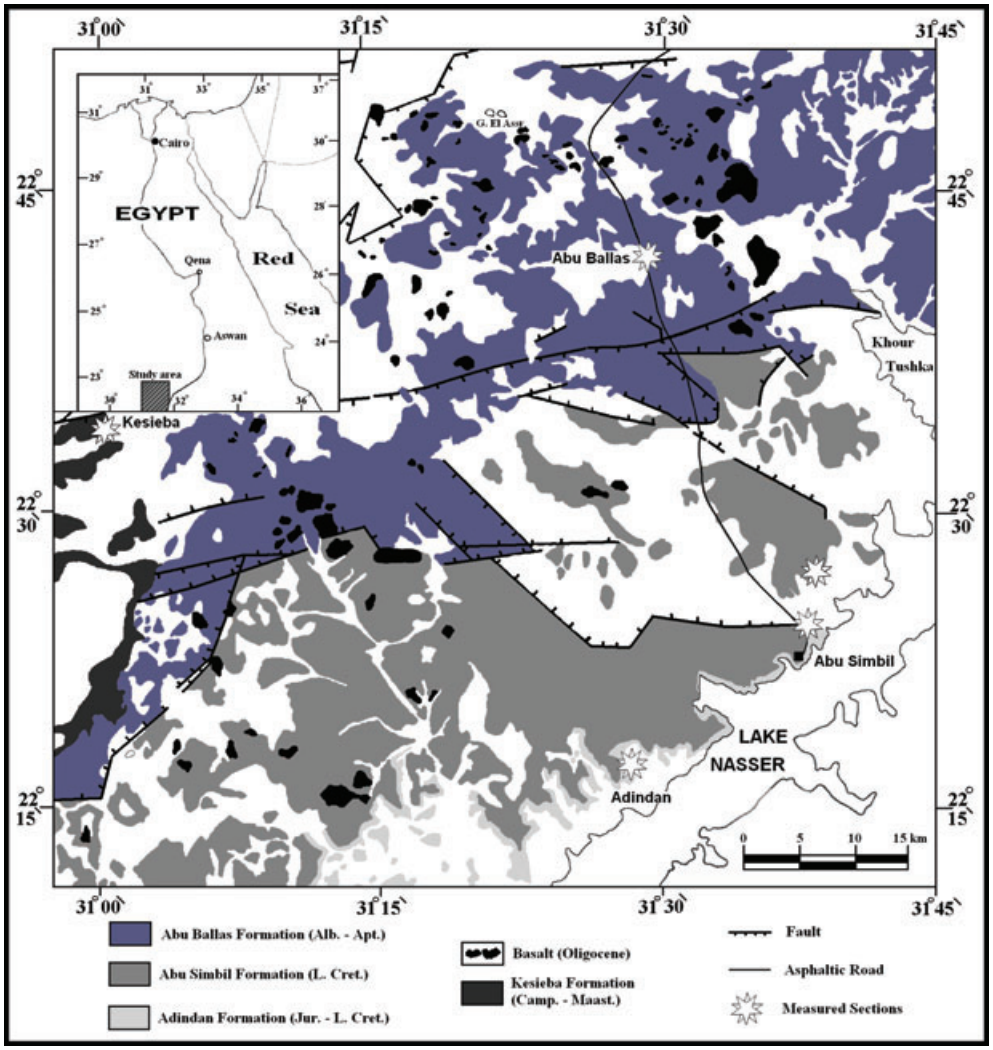

Figure 1. Location map of the studied Nubia Sandstone sections in Tushka area, south of Egypt (modified from EGPC-CONOCO 1987; Thabit 1994).

This target might be achieved by measuring the pore magnetic fabric of the studied rocks (Pfleiderer & Halls 1993; Durrast & Siegesmund 1999; Benson *et al.* 2003).

The spatial variation in the magnitude of the magnetic susceptibility with the different orientations of the rock is defined as the Anisotropy of Magnetic Susceptibility, AMS (Ising 1942). This property reflects the preferred orientation of magnetic minerals in rocks, that is, their magnetic fabrics. Such magnetic fabric has been found in full agreement with the petrofabric (Rathor 1975; Wood *et al.* 1976; Rochette *et al.* 1992; Tarling & Hrouda 1993).

Since AMS measurements constitute a second rank tensor, a magnetic anisotropy triaxial ellipsoid can be constructed; its orientation is described by $\chi_1 \geq \chi_2 \geq \chi_3$ which are its principal maximum, intermediate and minimum axes, respectively. Due to measurement speed, precision, low cost and range of applicability, AMS can be used adequately in petrofabric and structural studies (Hrouda 1982; Tarling & Hrouda 1993).

The AMS has been in particular used in the investigation of palaeocurrent in sedimentation basins, where relationships between the directions of principal susceptibility axes and sedimentary structures have been found in a good agreement (Hamilton & Rees 1970a,b).

According to Pfleiderer & Kissel (1994), variations of pore orientation, pore shape, porosity and permeability can be determined using magnetic pore fabric analysis. It is a technique developed for the study of 3-D orientation and shape anisotropy of connected pore spaces (Pfleiderer & Halls 1990, 1994; Pfleiderer & Kissel 1994; Hrouda *et al.* 2000; Benson *et al.* 2003; Benson 2004). These pores are injected with a magnetic suspension (ferrofluid) then measured for 'AMS' of pore spaces. Like grain fabric, maximum susceptibility will be parallel to the preferred direction of pore elongation. Any anisotropic shape of pore bodies will also cause anisotropy of magnetic susceptibility which in turn, helps in assessing the average shape and statistical alignment of pores (Pfleiderer & Halls 1993, 1994). The magnetic pore fabric technique is adapted to study sufficiently permeable rocks, that is, with permeability $K > 10^{-3}$ darcy (Pfleiderer & Halls 1990).

On the other side, porosity (Ø) is a ubiquitous feature of sedimentary rocks; it is defined as 'the percentage of pore volume to the total volume of the sample'. It originated from the fact that at the time of deposition the detrital grains are in tangential contact, leaving large empty volumes. As a result of precipitation and filling of the pore spaces and other diagenetic changes, porosity may be enhanced or decreased during geological history.

Downloaded from https://academic.oup.com/gji/article/177/1/43/729241 by guest on 26 June 2022

Laboratory experiments reveal that the major parameters enhancing porosity are dissolution and leaching of cement, fracturing and weathering, volume changes and recrystallization, as well as grain sorting, roundness and sphericity. In contrast, porosity is decreased by cementation and precipitation from hydrothermal solutions, the type, amount and distribution of the authigenic clay content, metamorphism, as well as orientation, packing and compaction with depth (Ragab *et al.* 2000). Porosity that evolves from the superposition of these processes exhibits a complex geometry and fabric. This is important, since the void space of rock and its geometry is a key control on other mechanical and physical properties, for example, Lo *et al.* (1986), Jones & Meredith (1998), Rasolofosaon & Zinszner (2002), Benson (2004), Benson *et al.* (2005), Louis *et al.* (2005) and Jones *et al.* (2006).

According to Levorsen (1967), porosity of reservoir rocks have been classified into: (1) negligible ($Ø \leq 5$ per cent), (2) poor ($5 < Ø \leq 10$ per cent), (3) fair ($10 < Ø \leq 15$ per cent), (4) good ($15 < Ø \leq 20$ per cent) and (5) very good ($20 < Ø \leq 25$ per cent).

Increasing the volume of the contained pore spaces (porosity) decreases values of the bulk density, which is controlled mainly by the mineralogical composition as well as by the pore spaces of rocks.

Permeability is mostly defined as 'the ability of the porous rocks to transmit fluids under certain pressure gradient', it is measured in darcy or m^2 (Pettijohn 1984). According to Pettijohn, permeability of consolidated rocks, is mostly influenced by: (1) the amount of the swelling clays; (2) the ability of the rock to retain the pore water *in situ* as irreducible water (Sw_{irr}); (3) channel diameter; (4) wettability; (5) porosity type and (6) tortuosity and complexity of channels (T).

According to Levorsen (1967), sedimentary reservoirs have been classified according to their permeability as: (1) fair ($1 < K \leq 10$ md), (2) good ($10 < K \leq 100$ md) and (3) very good ($100 < K \leq 1000$ md).

SAMPLING AND MEASURING PROCEDURES

Sampling has been carried out in 4 sites, the Adindan type section, the Abu Simbil type sections (two composite sections), the Abu Ballas section (on the Abu Simbil-Tushka way) and Kesieba section along Drab El Arbein-Tushka way (Fig. 1).

To reveal the mineralogical composition and to estimate the porosity values in 2-D and its types, a total of 86 fresh and non-weathered samples were collected in a representative sequence for the different lithological varieties (12 for Adindan Formation, 30 for Abu Simbil Formation, 38 for Abu Ballas Formation and 6 for Kesieba Formation). Then, for each sample two thin sections were prepared in two orthogonal directions, perpendicular and parallel to the bedding plane.

Impregnation with blue dye and staining with Alizarin Red-S were carried out for the thin sections to evaluate the present porosity and to differentiate the carbonates into dolomite and calcite minerals, respectively, using Dickson's technique (1966). Thin sections were studied for mineralogical analysis using polarized microscope and point counter to evaluate the percentage of the different components.

In addition, 5 fresh non-weathered samples were representatively selected out of these samples and coated with a thin layer of carbon and examined using the Scanning Electron Microscope (SEM). The SEM technique was applied to study and identify in details the types of pore spaces, the different mineralogical relationships, and types of clay minerals and their effect on the petrophysical properties.

Further 19 representative fresh block samples (neither weathered nor fractured) were collected from different lithologies and sequences (Fig. 2) and oriented in the field according to the bedding plane and to the magnetic north for the purpose of magnetic and petrophysical studies. Six to seven cylindrical samples per block were drilled vertically into 25 mm diameter by 22 mm length conforming the standard sample length/diameter ratio of 0.88 required for the AMS and pore fabric measurements (Banerjee & Stacey 1967; Noltimier 1971). A total of 125 core samples were then obtained for measuring the grain and pore AMS.

Due to the very low magnetic susceptibility of the studied samples, close to the noise level of the used bridge, measuring the anisotropy of magnetic grain susceptibility for the present samples was conducted using the Multi Functions Kappabridge (MFK1-FA). The bridge measures magnetic susceptibility along the 'z'-axis with a sensitivity of 10^{-8} SI units. Samples were sequentially rotated into 3 orthogonal orientations, with a measurement made in each orientation. Then the AMS ellipsoid could be characterized by its three principal magnetic susceptibility values (χ_1, χ_2, χ_3) and their orientation (declination and inclination values).

Following the recommendations of Ellwood *et al.* (1988) and Tarling and Hrouda (1993), the following set of parameters were

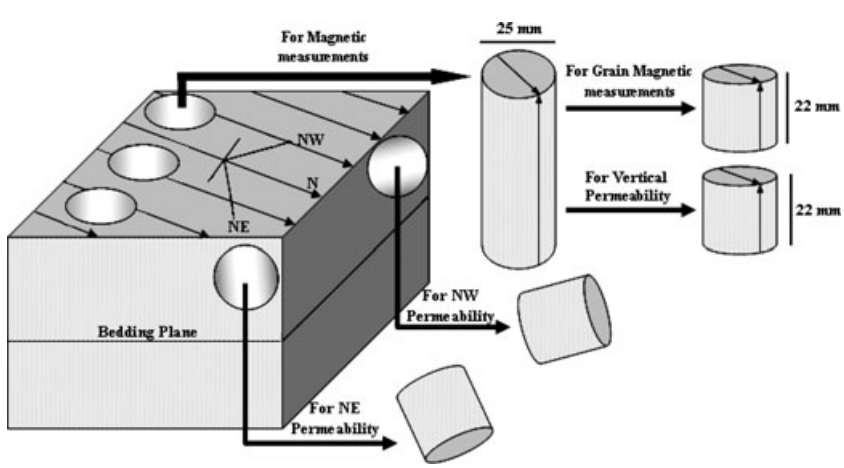

Figure 2. Coring procedure for both the magnetic and petrophysical fabric assignment.

Downloaded from https://academic.oup.com/gji/article/177/1/43/729241 by guest on 26 June 2022

used to define 'AMS' ellipsoid of rocks under study:

$\chi = (\chi_1 + \chi_2 + \chi_3)/3$	(Mean susceptibility, Nagata 1961)
$L_{mag} = \chi_1/\chi_2$	(Magnetic lineation, Balsley & Buddington 1960)
$F_{mag} = \chi_2/\chi_3$	(Magnetic foliation, Stacey *et al.* 1960)
$P_{mag} = \chi_1/\chi_3$	(Magnetic anisotropy, Stacey *et al.* 1960)
$T = [2 \ln(\chi_2/\chi_3)/\ln(\chi_1/\chi_3)] - 1$	(Ellipsoid shape, Jelinek 1981)
$q = (\chi_1 - \chi_2)/[(\chi_1 + \chi_2)/2 - \chi_3]$	(Shape parameter, Granar 1958)

The primary magnetic fabric parameters fall within specific ranges, such as $0.06 < q < 0.69$ and the 'imbrication angle', the angle between horizontal and the plane of maximum-intermediate susceptibility, is less than 20° (Rees 1966; Crimes & Oldershaw 1967; Hamilton & Rees 1970a, b; Rees & Woodball 1975). q-values outside these ranges can generally be attributed to coring disturbances, bioturbation and deformation. In addition, the depositional magnetic fabrics of most subaqueously deposited sediments are characterized by oblate susceptibility ellipsoids; therefore T, the shape parameter (Jelinek 1981), is strongly positive, usually approaching 1.0. When the value of T-parameter is negative ($-1 < T \leq 0$), it indicates tensional deformation giving rise to prolate ellipsoid.

In a trial to have more information about the magnetic carriers within these block samples, five samples were selected representing the studied formations and to determine their hysteresis properties using the MicroMag VSM in 1 Tesla maximum field.

Porosity (Ø) of the dry core-shaped samples was measured successively by two saturation methods using two fluids: (1) helium injection at 1.2 bar pressure using a helium pycnometer and (2) ferrofluid injection at 1 bar pressure using evacuation.

The bulk volume (V_b) and dry weight of 19 selected core samples (W_d) were measured using a precision caliper (0.1 mm precision) and an electronic balance (0.1 mg precision), whereas the grain volume (V_g) of the samples was measured using the helium pycnometer, and the following equation:

$$V_g = 34.989 + \frac{78.899}{1 - (P_1/P_2)},$$

where, P_1 and P_2 are the injection pressures and the relaxation pressure, respectively.

Three measurements were carried out for each sample and the final arithmetic mean was then calculated. The V_g is then substituted in the following equation:

$$Ø_{He} = 100 \times \frac{(V_b - V_g)}{V_b}.$$

Then after measuring the porosity using helium injection, the same 19 samples were evacuated using an evacuation chamber down to –1 bar (–101 kPa) and injected by a ferrofluid of density $\rho_{Fe} = 0.895$ g cm^{-3}. The ferrofluid or magnetic fluid is a stable colloidal solution of superparamagnetic magnetite nanoparticles (1–10 nm range) suspended in a solvent. Each particle is covered by insulating material to avoid coagulation of particles. The fluid behaved as a strongly magnetic homogeneous and isotropic media under the action of the magnetic field. Therefore, its magnetic anisotropy will directly reflect the shape of the injected pore spaces.

In order to avoid overloading sensitive susceptibility bridges, it is common practice to use diluted ferrofluid when studying high porosity rocks (e.g. Benson *et al.* 2003; Benson 2004). On the other side, Jones *et al.* (2006) approved a concentration threshold at approximately 50 per cent concentration below which the equivalent pore concept (EPC) method of Hrouda *et al.* (2000) ceases to work reliably. Hence, we used a 50 per cent ferrofluid concentration for the present AMS studies.

The ferrofluid-injected samples were weighed again in the saturation state (W_s) and their ferrofluid porosity ($Ø_{Fe}$) was then calculated using the following equation.

$$Ø_{Fe} = 100 \times \frac{(W_s - W_d)}{V_b \times \rho_{Fe}}.$$

Pore space-anisotropy of magnetic susceptibility (pAMS) for the present samples was then measured using the Kappabridge (KlY-2) magnetic susceptibility bridge. Samples susceptibility was measured in 15 different orientations. A least-square routine was then applied to fit a magnetic susceptibility ellipsoid to the data (Jelinek 1978).

Further additional 57 representative core samples were machined from the 19 block samples (3 samples/block) for permeability measurements. Since permeability measurements do not provide a second rank tensor, so the core samples were drilled in orthogonal directions (one sample taken vertical to the bedding plane, whereas the other two samples were drilled along the NE and NW directions within the bedding plane, Fig. 2). The choice of NE and NW directions were determined by the present magnetic pore fabric results. The length (L) the cross sectional area (A) of the core samples were measured using a caliper. Permeability measurement was conducted using a Ruska Gas permeameter; the core sample was introduced into a Hasler type core holder with the outer frame sealed to prevent bypass using pressure of 27.58 bar (400 psi). Dry nitrogen of viscosity μ was injected through the sample at a constant pressure. Taken into consideration the atmospheric pressure (P_a), the pressure difference between both sides of the sample (where P_1 is the upstream pressure and P_2 is the downstream pressure) and the flow rate (Q), permeability was then calculated using the following equation.

$$K = \frac{2000 \mu Q L P_a}{A\left(P_1^2 - P_2^2\right)}$$

LITHOSTRATIGRAPHY AND MINERALOGICAL COMPOSITION

The Nubia sandstones in their type sections in south Egypt have been studied by many authors, for example, Said (1962), Issawi (1973, 1978), Issawi & Jux (1982), Klitzsch (1979), Hermina *et al.* (1989), Hendriks (1988), Issawi & Osman (1993) and Thabit (1994).

From the field observations and taking into consideration the previous studies, the Nubia sandstones in their type sections and localities in southwest Egypt between latitudes 22°00′ and 22°45′N and longitudes 30°45′ and 31°45′ (Fig. 1) could be distinguished from top to bottom into five formations:

V.	Kesieba Formation	(Campanian–Maastrichtian)
IV.	Sabayia Formation	(Albian–Cenomanian)
III.	Abu Ballas Formation	(Aptian–Albian)
II.	Abu Simbil Formation	(Valanginain–Barremian)
I.	Adindan Formation	(Jurassic–Valanginain)

Downloaded from https://academic.oup.com/gji/article/177/1/43/729241 by guest on 26 June 2022

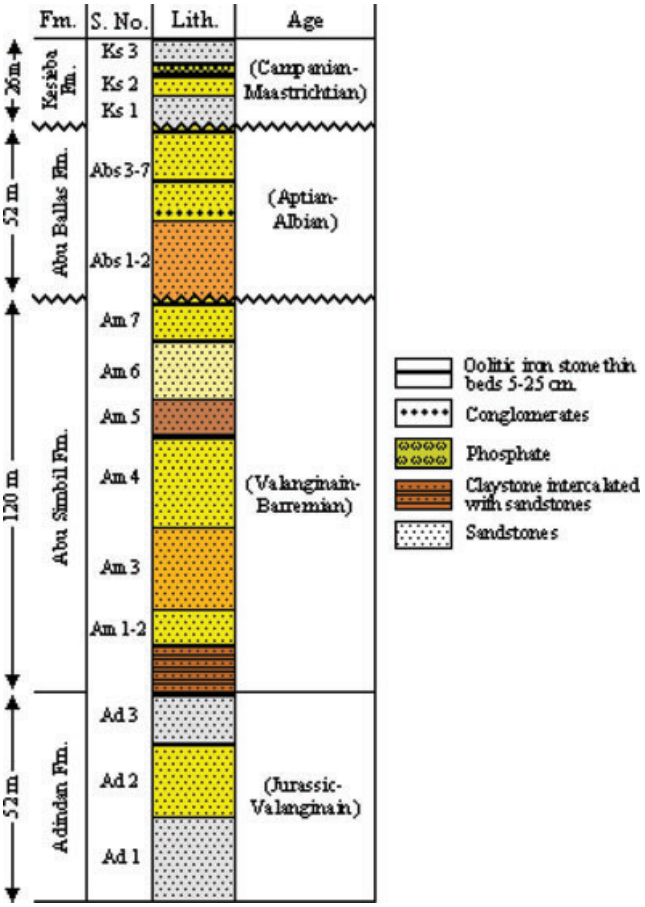

Figure 3. Schematic composite lithostratigraphic column of the Nubian sandstones in Tushka area, south Egypt.

Due to the significant deformation occurring after deposition of Sabayia Formation, it has been largely eroded in the studied area. Therefore, Sabayia Formation was not included in this study. From the field studies a composite lithostratigraphic column has been sketched for the studied Nubian formations (Fig. 3).

The Nubia sandstones have a more or less similar and homogeneous lithological composition through the entire sections in their type sections in Tushka. They show relatively little variation in depositional environment frequently accompanied with deposition of some oolitic ironstone beds at the top of each cycle of deposition (Fig. 4A) and some times filling joints and fractures. They are affected by many sets of joints and fractures (Fig. 4B), which may be attributed to tectonic events or to the arid weather. Several studies have dealt with the structural setting of Tushka area, for example, Mousa (1984), Thabit (1994) and ElSorady & Abdallah (2001).

According to Thabit (1994), the normal faults are the main structural features observed in the Tushka area; he arranged the observed faults in decreasing order of abundance as follows:

(1) E–W (N70°−90°E),
(2) N40°−50°E and N60°−70°E and
(3) N40°−50°W and N10°−20°W.

Petrographically, the Nubia sandstones are similar in composition through the different formations; they are composed of ill sorted, fine to coarse and rounded to angular quartz grains cemented together by silica cement, mostly represented as gravity/meniscus cement. Rare relics of calcite and sometimes fossil remains were

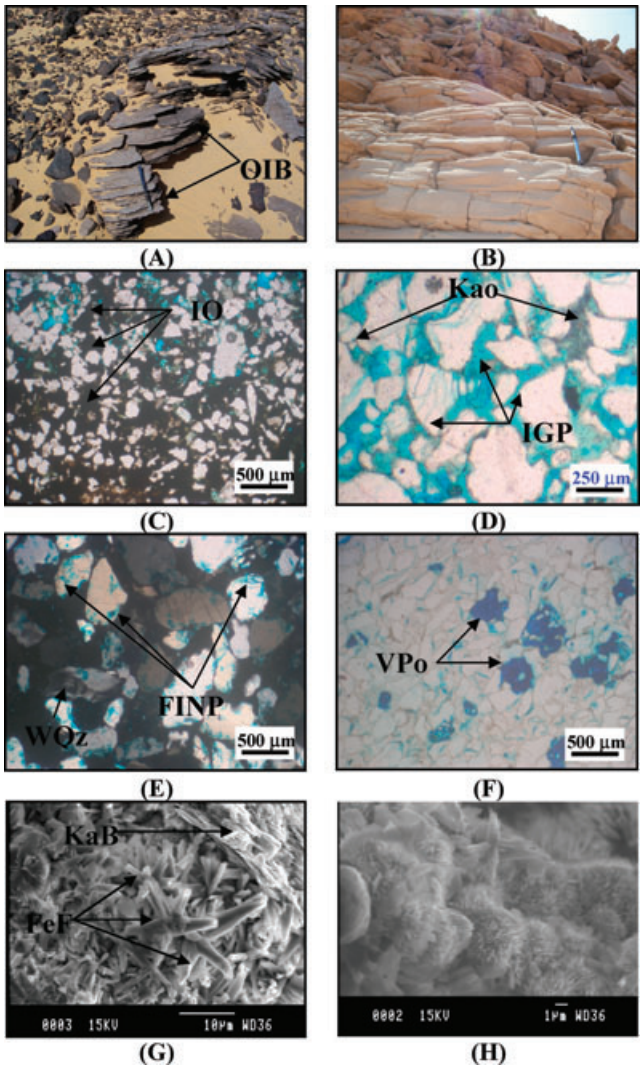

Figure 4. Photomicrographs of Nubian sandstones from type sections in south Egypt, the injected resin filling pores is dyed blue; (A) a banded oolitic ironstone (OIB) bed due to intensive tectonism, Abu Ballas Formation; (B) highly fractured blocky sandstones of Abu Ballas Formation. Panels (C)–(F) are photomicrographs show; (C) Much iron oxide patches (IO) masking micro/matrix and intergranular porosity, Abu Simbil Formation, PPL; (D) Much intergranular porosity (IGP). Some authigenic kaolinite booklets (Kao) partially filling pore spaces and cementing the quartz grains, the base of Abu Simbil Formation, PPL; (E) Intensive dissolution of quartz grains giving rise to skeletons of grains increasing the fracture and intragranular porosity (FINP) with some quartz grains have wavy extinction (WQz) due to compression forces, top of Adindan Formation, CN; (F) Angular to rounded quartz grains, with vuggy porosity (VPo), Adindan Formation, PPL. Panels (F) and (G) are SEM images show the characteristic structure of the iron oxides and clay content of the Nubia sandstones; (G) Some iron oxide filaments like sea stars (FeF) and some kaolinite booklets filling the pore spaces (KaB), top of Abu Simbil Formation and (H) Iron oxide accumulations in filament rose-like structure, top of Abu Simbil Formation.

noticed in Abu Ballas and Kesieba formations probably indicating that primary cement has been leached during diagenesis. The silica cement could be assigned as gravity cement and/or filling vuggy porosity. Cementation by silica was not sufficient to obliterate the high storage capacity of the present rocks, and just attached the grains together, sometimes slightly reducing porosity values. Some iron oxides, mostly as pigments (<5 per cent, Fig. 4C) and clay

Downloaded from https://academic.oup.com/gji/article/177/1/43/729241 by guest on 26 June 2022

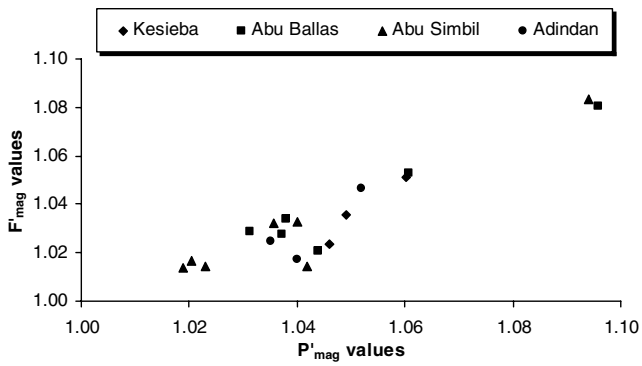

Figure 5. Corrected magnetic grain anisotropy (P'_{mag}) plotted versus the corrected magnetic foliation (F'_{mag}).

content (<5 per cent) are disseminated within the cement, partially filling and lining the pore spaces and sometimes cementing the quartz grains together (Fig. 4D).

The diagenetic history of the present sandstones seems to be complex and mostly obliterated. Cementation by silica is the most common feature; it is not uniform through the vertical and horizontal petrographical sections. Therefore, determination and comparison of porosity values in both the perpendicular and parallel directions to the bedding plane gave a detectable pore fabric's anisotropy. Porosity-decreasing diagenetic processes are mostly represented by compaction and pressure solution which have acted for a long time. However, the very good to excellent porosity values indicate that these processes were not efficient or compensated by the subsequent periods of dissolution and leaching out. The compaction and pressure solutions could be indicated by fractured quartz grains, sometimes internally deformed, with wavy extinction. The quartz grains are mostly in point contact, and sometimes in suture or concave–convex contact position (Fig. 4E).

On the other side, dissolution and leaching out are the main porosity-enhancing diagenetic factors giving rise to excellent porosity (Fig. 4F) and permeable paths for pore fluid movement. Following Levorsen's classification (1967), macro porosity measured on thin sections of the Nubia sandstones are ranked as good to very good. It varies between 20 and 35 per cent in the horizontal direction and between 15 and 25 per cent in the vertical direction indicating inhomogeneity in distribution of pore spaces. The pore spaces of the Nubia sandstone samples could be separated into: (1) intergranular porosity (Fig. 4D), (2) vuggy porosity (Fig. 4F), (3) fracture and intragranular porosity (Fig. 4E) and (4) matrix porosity, masked by the iron oxides (Fig. 4C).

Petrographically, investigation of pore fabric is not frequently applied, even though it may match the potential macro pores accessible by the economic fluids. Comparing the porosity values in both vertical ($Ø_V$) and horizontal ($Ø_H$) directions may introduce an over all view for the porosity anisotropy (λ_p) in these directions. By using the following equation, it was revealed that porosity anisotropy (λ_p) is ranging between 1.15 and 1.83 with average values equal to 1.30 for Adindan Formation, 1.52 for Abu Simbil, 1.20 for Abu Ballas Formation and 1.50 for Kesieba Formation.

$$\lambda p = \frac{\phi_H}{\phi_V}.$$

The obtained anisotropy values could be attributed mainly to the load pressure. Nevertheless, it is worth mentioning that, even though this petrographical tool can introduce an over all view on the anisotropy of pore space distribution in 2-D, it is unable to estimate the matrix/micro pores which may sometimes form more than 20 per cent percent of the total pore spaces. Moreover, the chaotic distribution of iron oxides and authigenic clay content in the pore spaces increase the inability of this tool to introduce a real estimation for the total pore spaces.

From the SEM studies, it could be stated that the clay content in the Nubia sandstone formations is represented mainly by authigenic kaolinite booklets filling the pore spaces (Fig. 4G), whereas the present iron oxide minerals are represented by hematite and sometimes goethite. The iron oxides exhibit filament rose- and sea star-like structures (Figs 4G and H:).

Following Ketzer *et al.* (2005), the kaolinite booklets of the Nubia sandstones have been formed *in situ* by diagenetic alteration of a probably smectitic precursor, which was mechanically infiltrated in the vadoze zone.

According to du Bernard & Carrio-Schaffhauser (2003), the occurrence of this type of clay cementation during early diagenesis can prevent or delay deep burial diagenetic processes and therefore preserve excellent reservoir properties.

MAGNETIC GRAIN FABRICS (PRE-INJECTION)

The studied sandstone samples showed rather similar magnetic grain fabrics through the whole sandstone sequence. With the exception of few sites, the original pre-injection magnetic susceptibility values are low to very low and homogeneous (Table 1). The combination of very low diamagnetic and para- or ferromagnetic susceptibilities may lead to inconsistent AMS ratios. This is clearly demonstrated by the largest anisotropy ratio are observed for the weakest mean susceptibility values. Therefore, we used the corrections proposed by Rochette (1987) and Rochette *et al.* (1992) for the diamagnetic susceptibility value as follows.

$$L'_{mag} = (L_{mag} \times \chi_2 + 1.4)/(\chi_2 + 1.4);$$

$$F'_{mag} = (\chi_2 + 1.4)/(\chi_2/F_{mag} + 1.4);$$

where $\chi_2 = (3 \times \chi_m)/(L_{mag} + 1 + 1/F_{mag})$ and

$$P'_{mag} = L'_{mag} \times F'_{mag},$$

where χ_m is the mean susceptibility values, L'_{mag} is the corrected magnetic lineation, F'_{mag} is the corrected magnetic foliation whereas P'_{mag} is the corrected magnetic anisotropy (Rochette 1987; Rochette *et al.* 1992, Fig. 5).

These corrections were proposed mainly for the magnetic susceptibility inducted from the quartz grains, which is the main component of Nubia sandstone samples. Such correction gave rise to more homogeneous data, particularly for the P and T values. Both the original uncorrected and the corrected grain fabric data are listed in Table 1.

The measured magnetic susceptibility, χ, ranges from 0.72 to 22.5×10^{-5} SI with the corrected anisotropy degree, P'_{mag}, varies from 1.019 to 1.096, L'_{mag} from 1.002 to 1.027 and F'_{mag} from 1.014 to 1.083 (Fig. 5). T-values indicate mostly planar fabrics, ranging between −0.313 (only three sites showed negative values) and 0.839, with P' for most sites being less than 1.05 (Fig. 6). On the other side, q-values vary from 0.101 to 0.988 with average 0.377, within the range of primary fabrics.

Hence, the studied AMS grain fabric mostly have magnetic anisotropy less than 5 per cent, positive T-values and q-values less than 0.69 indicating depositional foliated and primary fabrics which could be attributed to depositional currents. From the petrographical studies and the field observations, these fabrics could be attributed

Downloaded from https://academic.oup.com/gji/article/177/1/43/729241 by guest on 26 June 2022

Table 1. Pre-injection magnetic grain fabric data for the studied Cretaceous Nubia sandstones.

Formation	Site	χ	P_{mag}	P'_{mag}	L_{mag}	L'_{mag}	F_{mag}	F'_{mag}	T	T'	q	D_{max}	I_{max}	D_{int}	I_{int}	D_{min}	I_{min}
Kesieba formation																	
	Ks 3	7.64	1.071	1.060	1.010	1.008	1.061	1.051	0.716	0.711	0.158	39	2	309	0	216	88
	Ks 2	0.72	1.141	1.046	1.065	1.022	1.072	1.023	0.064	0.028	0.656	203	26	300	13	53	61
	Ks 1	1.52	1.053	1.049	1.025	1.013	1.070	1.035	0.048	0.457	0.636	72	2	163	25	337	64
Abu Ballas formation																	
	Abs 6	17.2	1.041	1.038	1.004	1.004	1.037	1.034	0.810	0.802	0.101	225	9	133	12	348	75
	Abs 5	22.5	1.102	1.096	1.015	1.014	1.086	1.081	0.703	0.694	0.691	112	11	204	10	337	75
	Abs 4	3.58	1.075	1.061	1.010	1.007	1.075	1.053	0.712	0.756	0.160	199	10	106	14	322	73
	Abs 3	2.27	1.052	1.031	1.004	1.002	1.047	1.029	0.829	0.839	0.092	174	12	265	3	8	78
	Abs 2	2.91	1.056	1.037	1.014	1.009	1.041	1.027	0.474	0.483	0.310	57	12	153	26	305	61
	Abs 1	0.90	1.117	1.044	1.058	1.023	1.055	1.021	−0.025	−0.043	0.714	191	7	93	46	287	43
Abu Simbil formation																	
	Am 7	2.59	1.063	1.040	1.011	1.007	1.051	1.033	0.629	0.636	0.210	32	7	126	24	287	65
	Am 6	4.88	1.046	1.036	1.004	1.003	1.042	1.032	0.82	0.822	0.096	196	1	106	15	288	75
	Am 5	11.1	1.024	1.020	1.004	1.004	1.019	1.017	0.618	0.650	0.213	145	6	235	3	351	83
	Am 4	2.61	1.064	1.042	1.042	1.027	1.022	1.014	−0.308	−0.313	0.988	215	17	120	16	350	67
	Am 3	0.83	1.051	1.019	1.013	1.005	1.038	1.014	0.491	0.479	0.298	191	18	88	35	303	49
	Am 2	2.33	1.157	1.094	1.016	1.010	1.138	1.083	0.776	0.776	0.127	247	1	337	3	139	87
	Am 1	0.98	1.057	1.023	1.020	1.008	1.036	1.015	0.273	0.275	0.454	209	11	300	6	59	77
Adindan formation																	
	Ad 3	15.8	1.038	1.035	1.011	1.010	1.027	1.025	0.42	0.417	0.345	9	0	99	7	276	83
	Ad 2	3.23	1.068	1.052	1.007	1.005	1.068	1.047	0.786	0.806	0.117	44	7	135	7	269	80
	Ad 1	2.13	1.067	1.040	1.037	1.022	1.029	1.017	−0.116	−0.126	0.789	44	6	134	0	224	84

Notes: χ , magnetic susceptibility $\times 10^{-5}$ SI units; P_{mag}, anisotropy degree; L_{mag}, magnetic lineation; F_{mag}, magnetic foliation; D_{max} and I_{max}, declination and inclination of K_{max}; T, ellipsoid shape; D_{int} and I_{int}, declination and inclination of K_{int}; q, shape parameter; D_{min} and I_{min}, declination and inclination of K_{min} and P', L', F' and T' are the corrected values for P, L, F and T, respectively.

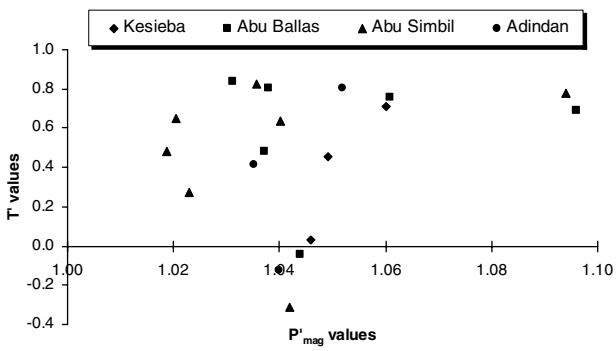

Figure 6. The corrected magnetic grain anisotropy (P'_{mag}) plotted against the corrected ellipsoid shape (T') values of the magnetic grain fabrics for the Nubia samples.

also to post diagenetic iron oxides-bearing hydrothermal activities invaded the Nubia sandstones. The invaded hydrothermal solutions dissolved and injected some iron oxides into the pore spaces as a diagenetic component, stained the quartz grains and mostly led to dissolution of feldspars and quartz grains leaving behind skeletons of exhausted quartz and some authigenic clay content (Figs 4G and H:). Although some hand samples are brownish-coloured and accumulations of some iron oxides could be noticed petrographically, the studied samples have very low to low magnetic susceptibility indicating a staining by hematite in the studied samples rather than accumulation of important volume of iron oxide.

The plot of stratigraphic height against the corrected magnetic lineation, foliation and the magnetic anisotropy (Fig. 7), shows a similarity between curves of both the magnetic foliation and anisotropy, but no comparable relation with the magnetic lineation. There are no systematic changes of the magnetic fabric parameters with increasing height. This plot together with the X–Y plot of $F'_{mag} - P'_{mag}$ ensures that the magnetic foliation is the main contributor to the magnetic anisotropy. In other words, the compaction due to the load pressure was not enough for controlling the obtained magnetic anisotropy; it was only the continuous injection by hydrothermal solution.

The corrected pre-injection maximum, intermediate and minimum grain magnetic susceptibility directions were plotted on the equal area lower hemisphere stereographic plots as in Fig. 8. It shows well-grouped vertical minimum susceptibility axes and a more or less consistency of the maximum susceptibility directions for the Adindan Formation along the NE–SW direction, which may be used as an indication of fluvial deposition through a palaeocurrent flowing mostly in this direction (Fig. 8A).

Plotting χ directions for both Abu Simbil and Abu Ballas formations, show similar behaviour (Figs 8B and C,). Both show a good distribution of the maximum and intermediate magnetic susceptibility directions along the bedding plane with imbrication angle $\leq 20^\circ$ and clustering of χ_{min} that were slightly deviated and elongated in the NW–SE direction, indicating a palaeocurrent has flowed in the NE–SW direction perpendicular to the deviated χ_{min} clustered directions. This deviation is due to the deposition by palaeocurrent of relatively high speed causing rolling the grains in the NW–SE direction.

Upwards at the top of the studied section, Kesieba Formation (Campanian–Maastrichtian) shows a return into the relatively quiet palaeocurrent conditions prevailing at the base of the Nubia sandstones with again a good clustering of χ_{min} around the vertical axis and scattering the maximum susceptibility directions along the bedding plane (Fig. 8D). The distribution of the magnetic susceptibility directions indicates the same palaeocurrent direction, NE–SW, stated for Adindan Formation.

© 2009 The Authors, *GJI*, **177,** 43–61
Journal compilation © 2009 RAS

Downloaded from https://academic.oup.com/gji/article/177/1/43/729241 by guest on 26 June 2022

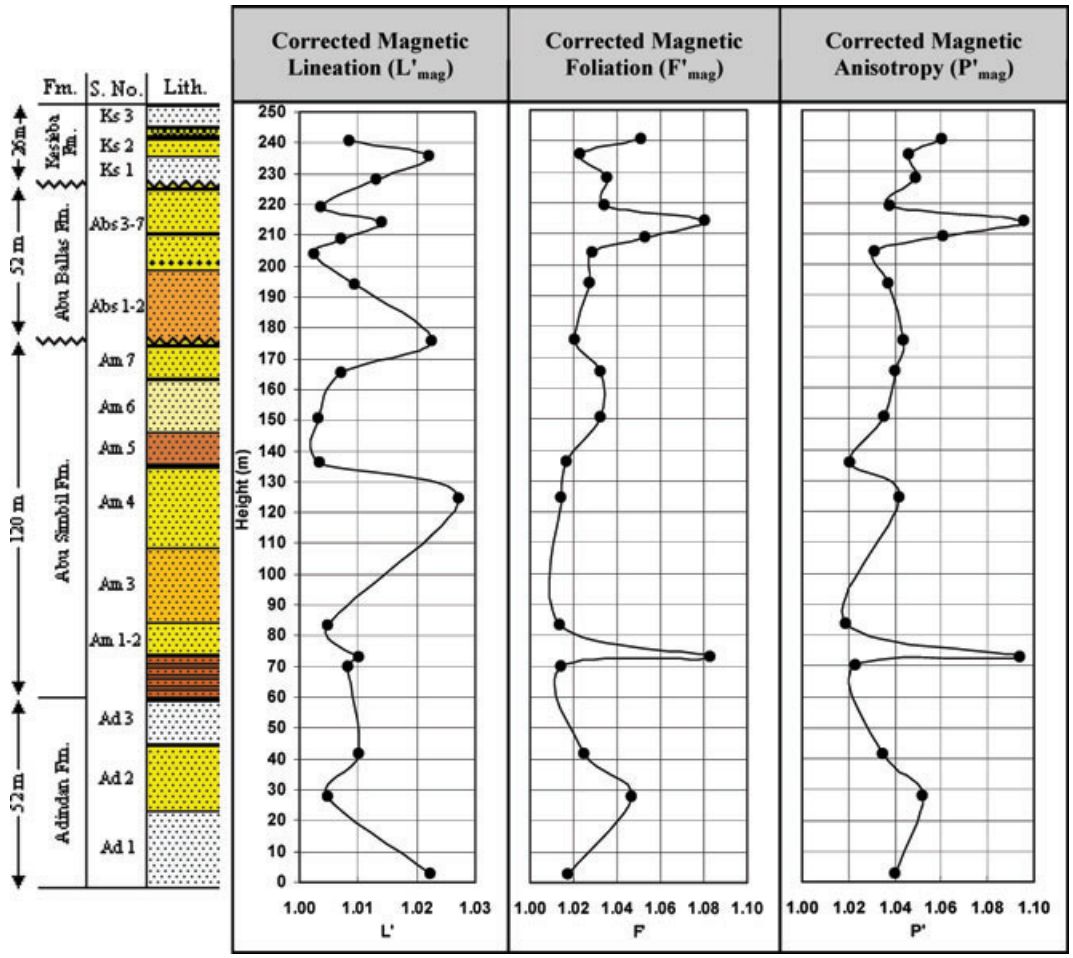

Figure 7. Vertical matching and correlation of the corrected magnetic grain parameters for pre-injection fabrics of the Nubia sandstones.

The imbrication angles for the different plots (≤20°) indicate a more or less horizontally and non-tilted fabrics through the entire sequence of the studied Nubia sandstone (Fig. 8), which reveals a gentle slope fluvial to deltaic regional system.

Therefore, it could be concluded that a regional palaeocurrent flowing mostly in the NE direction was responsible for deposition of the Nubia sandstone formations in Tushka area; this palaeocurrent had a more or less gentle slope, may be due to deposition into a delta system. In addition, the relatively higher speed of the palaeocurrents prevailed during the deposition of both Abu Simbil and Abu Ballas formations may indicate a sea regression phase during this period.

Finally, the magnetic carriers of the magnetic grain fabrics of the Nubia Sandstones were determined in five selected samples by hysteresis measurements. The low and high field magnetic susceptibility values reveal that the magnetic susceptibility is mainly carried by the ferromagnetic grains, which therefore likely dominate also magnetic anisotropy. High field susceptibility is diamagnetic (quartz) in two samples and paramagnetic (clays and goethite) for the other level in Abu Simbil samples. The hysteresis parameters after high field slope correction points clearly to hematite or goethite: M_{rs}/M_s ranges from 0.35 to 0.75, B_{cr}/B_c from 1.3 to 6.1 with B_{cr} from 185 to 556 mT. Then "saturation" remanence (in 3 Teslas) was demagnetized firstly at 120 °C, then at 120 mT. It clearly points to goethite–hematite mixture in Adindan Formation, dominant hematite in Abu Simbil samples and dominant goethite in the Abu Ballas-Kesieba sequence.

PORE NETWORK FABRICS (POST-INJECTION)

A number of techniques have been proposed that aim directly to measure pore space geometry. In this study, we tend to approach the investigation of the void geometry in two different but interlinked methods; magnetic and petrophysical pore fabric techniques.

The helium porosity ($Ø_{He}$) of the studied samples varies between 25.8 and 40.8 per cent with an average of 33.5 per cent (Table 2). Then, later to the injection process, the ferrofluid porosity ($Ø_{Fe}$) was determined; it varies between 19.8 and 34.5 per cent of average 26.7 per cent.

The measured $Ø_{He}$ values were plotted versus the measured $Ø_{Fe}$ (Fig. 9); it indicates a good direct proportional relationship between both data. This relationship could be expressed in a linear equation as follows.

$$Ø_{Fe} = 0.90 Ø_{He} - 3.53 \quad (r = 0.80).$$

On the other side, the mean bulk density values could be related to the helium porosity values measured ($r \geq -0.77$) rather than that measured by ferrofluid injection ($r \leq -0.69$, Fig. 10).

Ferrofluid injection

$$Ø_{Fe} = -19.81\rho_b + 64.18 \quad (r = -0.69).$$

Helium injection

$$Ø_{He} = -18.37\rho_b + 68.83 \quad (r = -0.77)$$

Downloaded from https://academic.oup.com/gji/article/177/1/43/729241 by guest on 26 June 2022

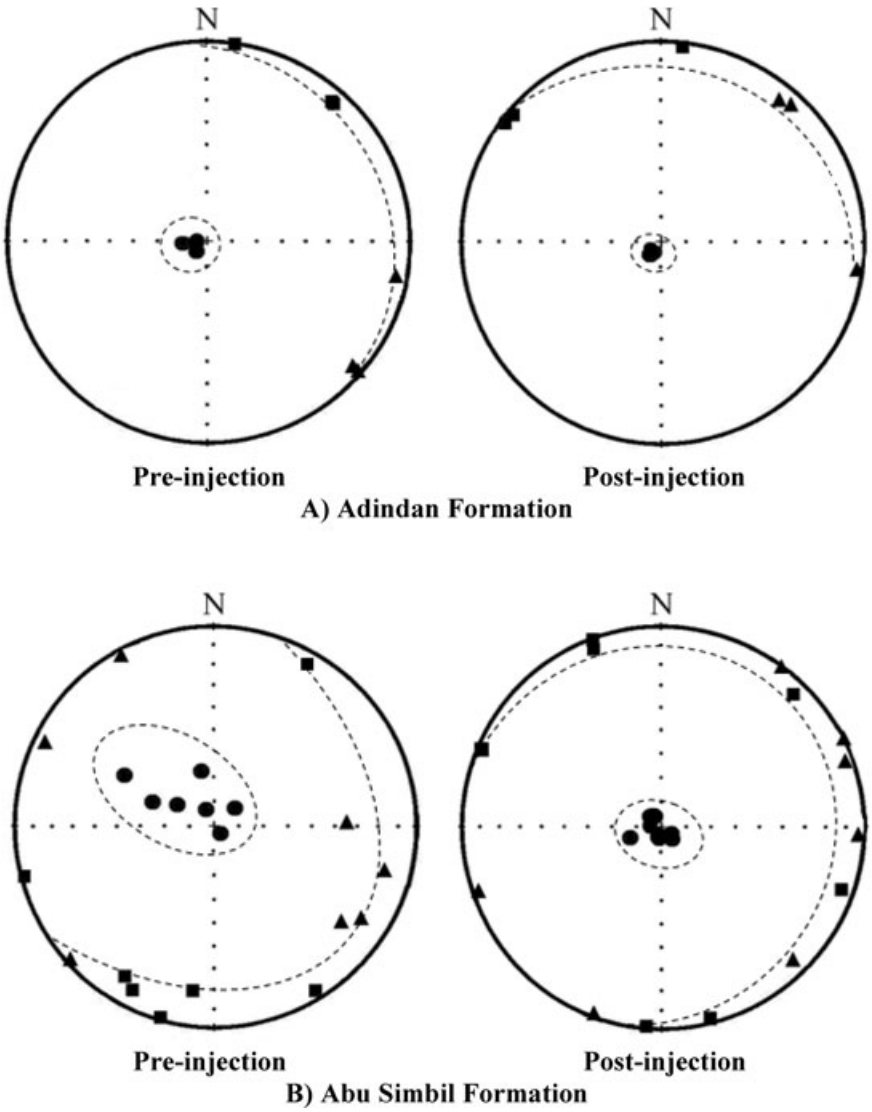

Figure 8. Equal area lower hemisphere stereographic plots for the corrected maximum (squares), intermediate (triangles) and the minimum (circles) grain magnetic susceptibility directions for the pre- and post-injection fabrics of the Nubia sandstones. The dashed curves pass through the maximum and intermediate magnetic susceptibility plots, indicating the imbrication angle, whereas the dashed lines surrounding the minimum values illustrate the clustering of χ_3 plots.

In a trial to follow up the changes in bulk density and porosity against height, bulk density and porosity values measured by the different techniques at the low and high-pressure injections were plotted against height (Fig. 11). Both the density and porosity curves show a good correlation with height. Porosity values decrease upward, whereas the density increases upward in a cyclic behaviour between the formations. In addition, there is image mirror behaviour between the plot of the bulk density and the measured porosity values indicating main contribution of the bulk density by the pore spaces. Although the measured porosity data is correlative in the low and high-pressure conditions, a detectable difference between the vertical tracing of both types was detected (7–15 per cent) particularly at the lower and top parts.

So a question that could be raised is: why there is a difference between the two determined porosity values for the same rock sample? The main reason is the presence of micro pore throats of diameter less than that of the ferrofluid suspension, so the ferrofluid molecules cannot pass through and a number of dead pores will be raised. The fact that helium injection better measures the total porosity is reflected by its better correlation with bulk density.

The post-injection magnetic susceptibility/magnetic permeability values are relatively high to very high, and vary from 7.53 to 13.1×10^{-2} SI of average 10.4×10^{-2} (Table 2). These high χ_{pore} values could be attributed to the very high porosity values, that is, much more invasions by the ferrofluid through the pore spaces. Both porosity data were then plotted versus the raised post-injection magnetic susceptibility, χ_{pore} (Fig. 12). As it is expected, the relationship between the ferrofluid porosity and χ_{pore} is more reliable than that with the $Ø_{\text{He}}$. Two empirical equations were introduced presenting the $Ø$–χ_{pore} relationship as follows.

$$\chi_{\text{pore}} = 0.26Ø_{\text{He}} + 1.80 \quad (r = 0.62)$$

$$\chi_{\text{pore}} = 0.33Ø_{\text{Fe}} + 1.61 \quad (r = 0.90).$$

In a similarity to the pre-injection case, the data plot against height indicates a better match between the χ_{pore} and $Ø_{\text{Fe}}$ rather than that with $Ø_{\text{He}}$ (Fig. 11). The presence of a good similarity between χ_{pore}, $Ø_{\text{He}}$ and $Ø_{\text{Fe}}$ logs in the height range of 80–200 m (Abu Simbil-Abu

© 2009 The Authors, *GJI*, **177,** 43–61
Journal compilation © 2009 RAS

Downloaded from https://academic.oup.com/gji/article/177/1/43/729241 by guest on 26 June 2022

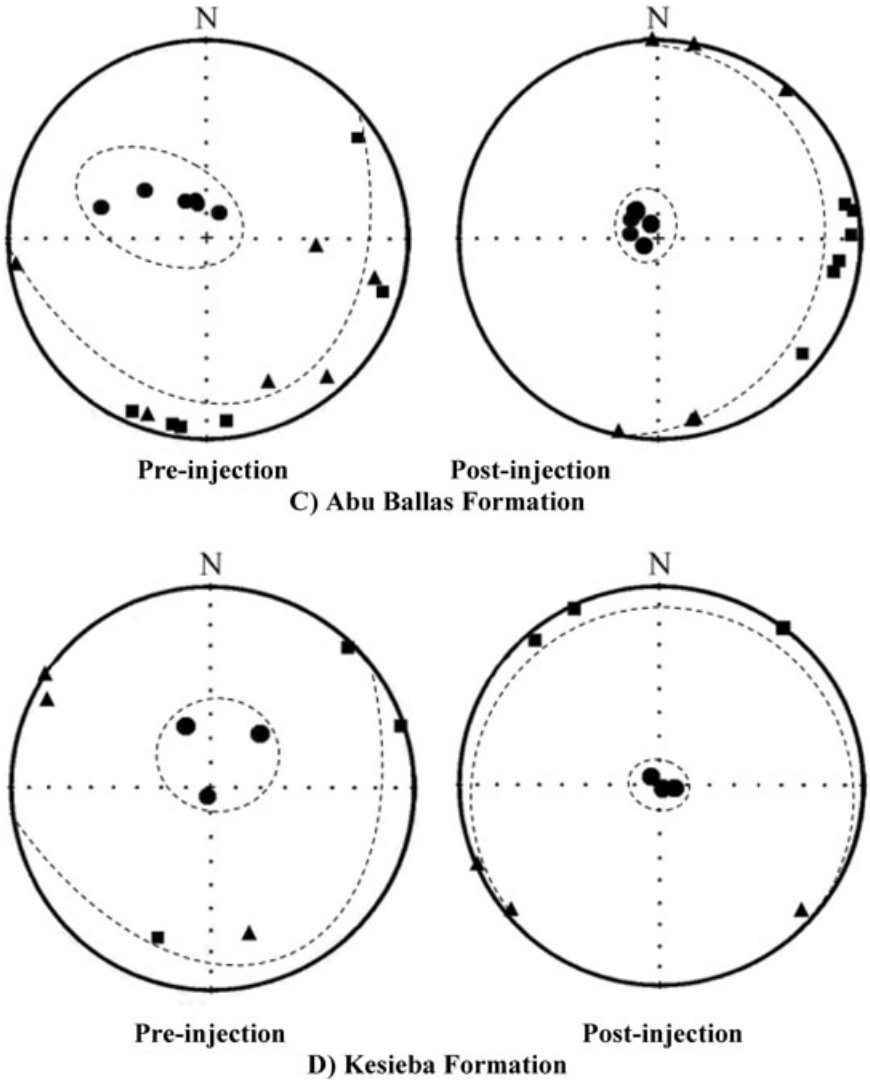

Figure 8. (*Continued.*)

Ballas sequence) indicates homogeneity in distribution of the micro pore throats, which are not accessible to the injected ferrofluid.

The post-injection anisotropy degree (P_{mag}) varies from 1.017 to 1.036, L_{mag} varies from 1.002 to 1.010 and F_{mag} from 1.013 to 1.034. These values are relatively lower than that assigned for the pre-injection magnetic grain fabric, but have more reliability due to the relatively high to very high post-injection χ_{pore}.

Similar to the magnetic grain fabric, the magnetic anisotropy of the Nubia sandstones is strongly planar (Fig. 13). T varies between 0.42 and 0.87 with no (Fig. 14), indicating predominance of the foliated pore fabrics. In addition, q-values vary from 0.069 to 0.344 with average 0.147, which is diagnostic for primary fabrics.

Plotting the magnetic lineation, foliation and magnetic anisotropy against height, shows a typical similarity between both curves of the magnetic foliation and anisotropy, with no contribution to the magnetic lineation (Fig. 15). This plotting together the X–Y plot of F_{mag}–P_{mag} relationship ensures that the magnetic pore foliation is the main contributor of the pore magnetic anisotropy. The compaction due to the load pressure was not strong enough to control the foliation of these pores.

The equal area lower hemisphere stereographic plots of the post-injection maximum and minimum magnetic pore susceptibility directions are shown in Fig. 8. It shows a better clustering of the minimum axes around the vertical axis than the pre-injection magnetic grain fabric and less scattering of the maximum pore elongation through the bedding plane. Adindan Formation at the base of the Nubia sandstones shows pore elongation swinging around the NNW direction (Fig. 8A). The pore fabric elongation of Abu Simbil shows more scattering through the NW, NE and SE direction with main direction referring to the NE one (Fig. 8B).

Plotting the principal χ_{pore} axes for Abu Ballas Formation (Aptian–Albian), shows a case different from the lower two formations. The pore elongation is mainly clustered around the East direction, which is one of the main fault trends in Tushka area as revealed by many authors, for example, Issawi (1978), Mousa (1984), Thabit (1994) and El-Sorady & Abdallah (2001). So, it is believed that the magnetic permeability (pore elongation) of Abu Ballas Formation follows the main fault trend in the study area to the E–W (Fig. 8C). The pore fabric elongation through Kesieba Formation at the top of the Nubia sequence is similar to that obtained for Adindan Formation at the base; it varies around the NNW direction (Fig. 8D).

After measuring the magnetic pore fabric we cored the block samples again in three orthogonal directions, one vertical

Downloaded from https://academic.oup.com/gji/article/177/1/43/729241 by guest on 26 June 2022

Table 2. Post-injection pore magnetic fabric data for the Nubia sandstones.

Formation	Site	χ_{pore}	P_{mag}	L_{mag}	F_{mag}	T	q	D_{max}	I_{max}	D_{int}	I_{int}	D_{min}	I_{min}	ρ_b	$Ø_{He}$	$Ø_{Fe}$
Kesieba formation																
	Ks 3	8.55	1.034	1.003	1.031	0.813	0.100	39	1	129	7	300	83	2.000	29.1	23.2
	Ks 2	8.99	1.019	1.002	1.017	0.769	0.124	335	2	245	0	153	88	2.193	30.9	23.4
	Ks 1	7.53	1.029	1.004	1.024	0.708	0.160	321	4	230	3	102	85	2.157	31.1	19.8
Abu Ballas formation																
	Abs 6	12.2	1.027	1.004	1.023	0.700	0.164	129	14	38	3	297	76	1.840	35.5	33.3
	Abs 5	11.8	1.024	1.002	1.021	0.797	0.108	78	1	168	7	342	83	2.030	36.0	30.1
	Abs 4	12.6	1.017	1.004	1.013	0.559	0.250	89	5	359	1	263	85	1.820	34.6	30.5
	Abs 3	8.65	1.020	1.003	1.017	0.703	0.162	76	6	167	9	310	79	1.900	30.0	22.9
	Abs 2	12.3	1.036	1.003	1.033	0.845	0.082	104	12	195	2	294	78	1.754	35.8	31.3
	Abs 1	10.4	1.020	1.003	1.017	0.716	0.154	100	12	10	0	279	78	1.709	38.5	26.9
Abu Simbil formation																
	Am 7	13.1	1.024	1.003	1.021	0.765	0.126	305	1	35	2	196	88	1.664	40.6	34.1
	Am 6	9.14	1.035	1.003	1.032	0.803	0.105	45	10	136	6	256	78	2.016	29.6	23.2
	Am 5	12.3	1.028	1.002	1.026	0.843	0.083	184	1	94	3	298	86	1.870	36.5	31.9
	Am 4	8.72	1.036	1.002	1.034	0.865	0.071	336	2	246	2	106	87	1.990	33.0	22.0
	Am 3	11.3	1.019	1.003	1.017	0.686	0.172	161	2	71	4	276	85	1.739	38.4	30.0
	Am 2	9.97	1.018	1.004	1.015	0.586	0.233	111	4	202	1	311	86	1.825	33.5	24.7
	Am 1	10.1	1.034	1.010	1.024	0.420	0.344	333	7	63	0	156	83	1.682	37.8	29.2
Adindan formation																
	Ad 3	9.86	1.024	1.003	1.022	0.779	0.118	7	4	97	2	217	85	2.040	28.9	20.7
	Ad 2	11.1	1.017	1.003	1.014	0.682	0.174	311	1	41	5	213	85	1.920	30.3	23.8
	Ad 1	9.75	1.029	1.002	1.027	0.869	0.069	307	2	37	6	201	84	1.816	36.8	25.9

Notes: χ_{pore}, post-injection magnetic permeability $\times 10^{-2}$ SI units; ρ_b, the bulk density in g cm^{-3}; $Ø_{He}$, porosity measured by helium injection; and $Ø_{Fe}$, porosity measured by ferrofluid injection. Other denotations as in Table 1.

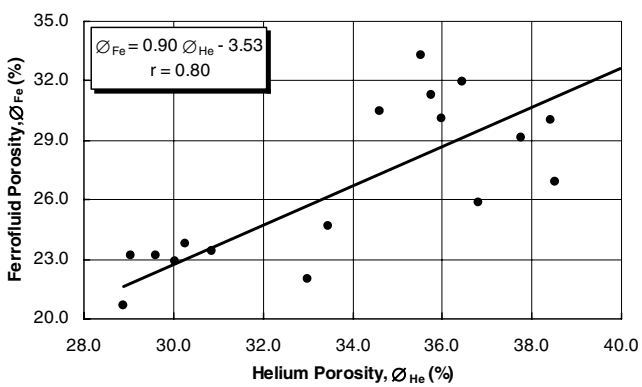

Figure 9. Measured ferrofluid porosity ($Ø_{Fe}$) plotted versus the helium porosity ($Ø_{He}$).

and one along the average pore elongation for permeability measurements.

According to Levorsen's (1967) classification for permeable reservoir rocks, the permeability values of the Nubia sandstones correspond to very good permeable rocks varying from 109 to 7750 mD (Table 3). The measured bulk permeability values (K_b) could be correlated to the helium porosity values (Fig. 16) better than with the ferrofluid porosity values. This highlights the role of some micro permeable pore spaces.

$$\text{Log } K_b = 9.44Ø_{He} - 11.37 \quad (r = 0.77).$$

The given empirical equation, nevertheless, only satisfies the permeability-porosity relationship for the Abu Simbil and Abu Ballas samples which indicates chaotic distribution of the micro pore spaces and pore throats in both Adindan and Kesieba samples.

The mean permeability values were plotted against height in Fig. 11. K-values could be correlated with height, where it decreases upward, in a cyclic behaviour between the formations with the highest values in top most parts of Abu Ballas Formation, which may be attributed to some structural control factors in this formation.

Due to increasing the compaction and load pressure effect with the geologic times, the vertical permeability values are expected to be lower than that measured for samples cored in the bedding plane direction. Some samples (Ad 3, Am2, Abs 3, Abs 4 and Abs 6) have vertical permeability values higher than the horizontal permeability (Table 3), which could be attributed to fracture permeable porosity dominated in the vertical direction.

Permeability values for both Adindan and Kesieba samples are mostly higher in the NW–SE direction, whereas for Abu Simbil samples are higher in the NE–SW direction, which is in consistent with the pre-measured magnetic data.

The measured values for Abu Ballas refer to a direction swinging between NE–SW and NW–SE as a main flow direction for half the samples, whereas the other samples have the highest permeability in the vertical direction, that is, indicate presence of some permeable fractures. On the other side, the magnetic pore fabric data of Abu Ballas Formation refers to a pore elongation extended in the E–W direction. From the structural studies, Abu Ballas Formation has suffered many structural events separated it from the underlying Abu Simbil Formation and caused the removal of the overlying Sabayia Formation from most places in Tushka area and brought the Kesieba Formation in disconformity position against it.

Following Nabawy and El-Hariri (2008), measuring permeability in three orthogonal directions enabled us to match the pore spaces in the 3-D, that is, to define their anisotropy, elongation and foliation. Achieving this target, we tend to use the following terms in this study.

'Petrophysical pore elongation' (E_{pet}) characterizes the most preferred direction for interstitial fluid migration and could be defined as 'the ratio between the maximum and the intermediate

Downloaded from https://academic.oup.com/gji/article/177/1/43/729241 by guest on 26 June 2022

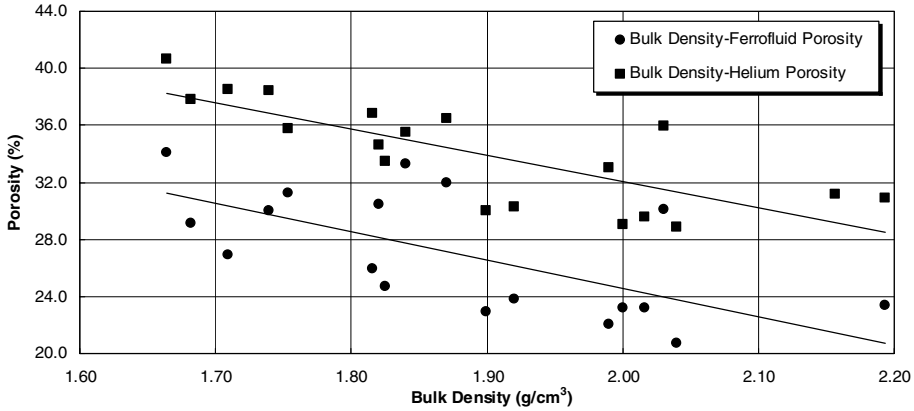

Figure 10. *X–Y* plot of bulk density against porosity values measured by ferrofluid and helium injection.

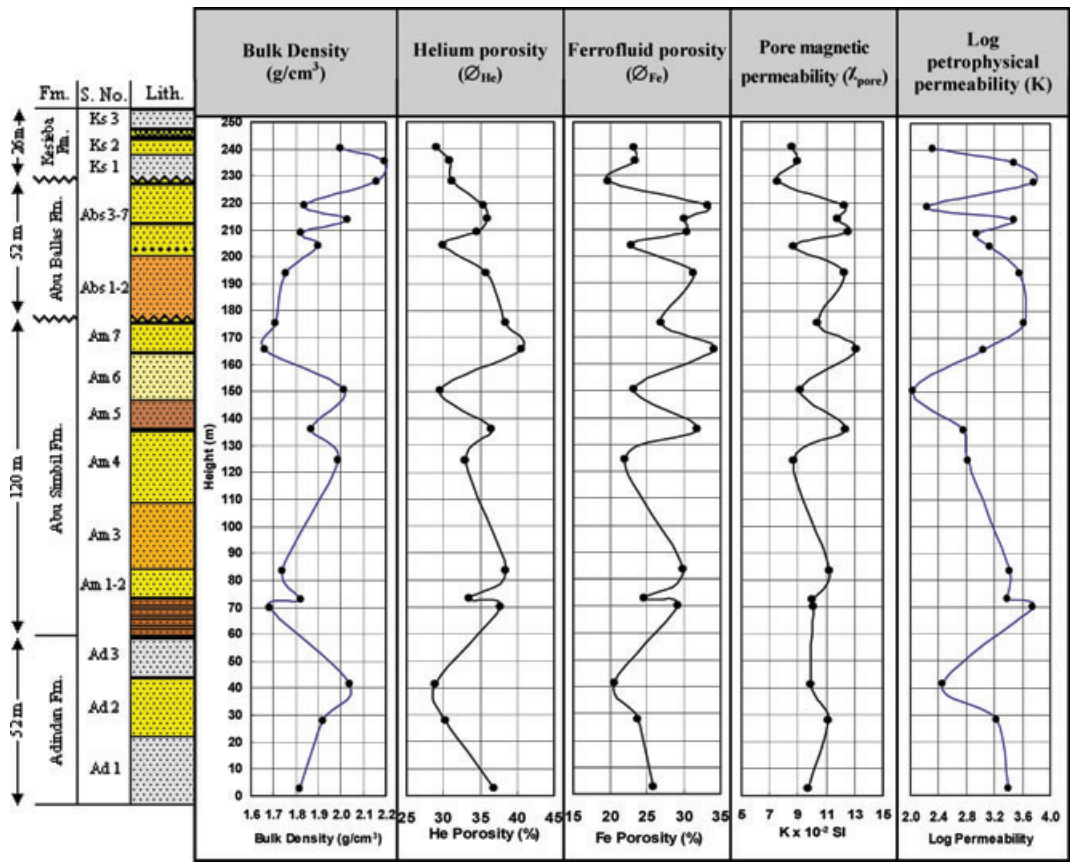

Figure 11. Vertical matching of the measured density, mean permeability, the post-injection magnetic permeability (χ_{pore}), and both types of porosity ($Ø_{\text{He}}$ and $Ø_{\text{Fe}}$).

permeability values'.

$$E_{\text{pet}} = K_{\max}/K_{\text{int}}.$$

'Petrophysical pore foliation' (F_{pet}), on the other side, is a term used to characterize the plane perpendicular to the flow direction, it is 'the ratio between the intermediate and minimum permeability values'.

$$F_{\text{pet}} = K_{\text{int}}/K_{\min}.$$

The current flow within the rock body in the 3-D is controlled mainly by the pore elongation and foliation which in turn are controlled by the pore throat distribution and its complexity, by tortuosity of the pore channels and by the presence of swelling authigenic clay minerals. This may reveal the pore phase distribution in the 3-D, that is, the 'petrophysical pore fabric'. It is a term refers to 'the pore distribution and pore anisotropy (λ_{pet}) in the 3-D, it is a resultant vector of the pore elongation and foliation'.

$$\lambda_{\text{pet}} = (E_{\text{pet}} \times F_{\text{pet}})^{1/2} = (K_{\max}/K_{\min})^{1/2}.$$

The petrophysical pore anisotropy is a real measure for the easiness of transmission fluids in the flow paths in the 3-D. The measured petrophysical pore elongation, foliation and anisotropy are listed in Table 3. To avoid pseudo presentation of these relations and having unrepresentative empirical equations, some anomalously high

Downloaded from https://academic.oup.com/gji/article/177/1/43/729241 by guest on 26 June 2022

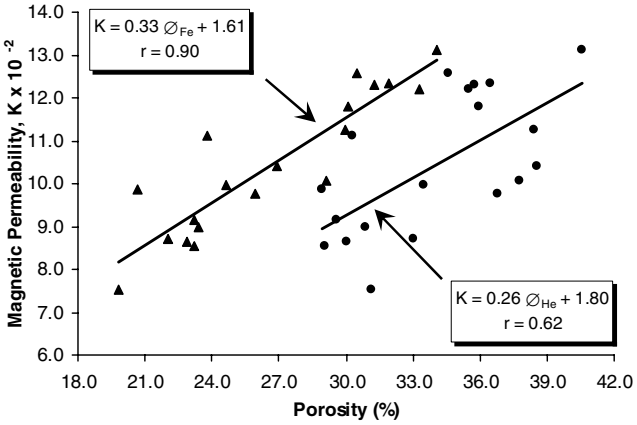

Figure 12. The post-injection magnetic permeability ($\chi_{\text{pore}} \times 10^{-2}$) of the Nubia sandstones is mainly dependant upon ferrofluid porosity ($Ø_{\text{Fe}}$) rather than helium porosity ($Ø_{\text{He}}$).

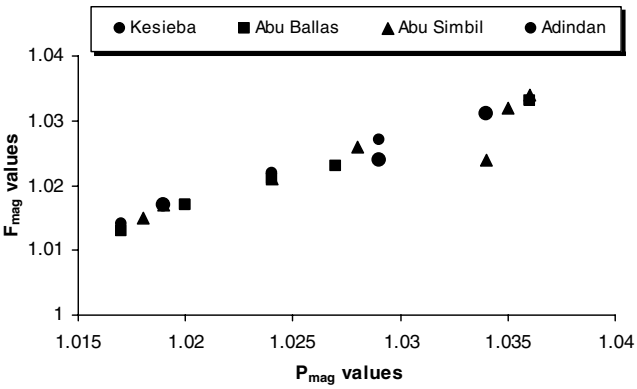

Figure 13. Plot of the magnetic pore anisotropy (P_{mag}) versus the magnetic pore foliation (F_{mag}).

anisotropy values were excluded away from the processing, for example, Am 6, Abs 5 and Ks 3. Therefore, the Nubia sandstone pore spaces have anisotropy values mostly vary from 1.06 to 1.80, pore foliation varies from 1.04 to 2.06 and the pore elongation varies from 1.02 to 1.61 (Table 3). Anisotropy of pore spaces (λ_{pet}) is mainly contributed by the pore foliation rather than the pore elongation (Fig. 17). From this study, some empirical equations could be used to calculate the anisotropy of pore spaces in terms of their elongation and foliation as follows.

$$\lambda_{\text{pet}} = 0.63E_{\text{pet}} + 0.45 \quad (r = 0.66)$$

$$\lambda_{\text{pet}} = 0.49F_{\text{pet}} + 0.61 \quad (r = 0.80).$$

The anisotropy values of the measured permeability were plotted against the height Fig. 15. Comparing the permeability anisotropy parameters indicate that the petrophysical pore anisotropy is mostly attributed to the pore foliation rather than pore elongation, particularly through the Abu Simbil and Abu Ballas sequence.

GENERAL DISCUSSION

The initial magnetic susceptibility of the Nubia sandstones is low to very low and mainly carried by diamagnetic (quartz) and antiferromagnetic minerals (hematite and goethite; Figs 4G and H:). These magnetic carriers were detected by studying the hysteretic loops of the studied samples. High field susceptibility is diamagnetic (indicating quartz) for most samples, whereas the hysteresis parameter with very high co-ercivity points clearly to hematite or goethite.

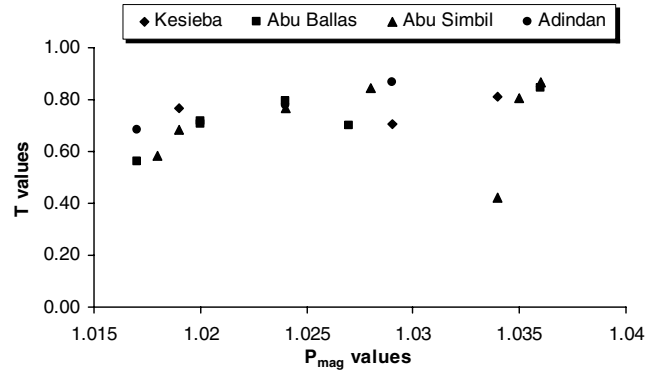

Figure 14. Plotting the magnetic pore anisotropy (P_{mag}) against the ellipsoid shape (T) values.

The ferrofluid injection process was very reliable due to the excellent porosity and permeability values of the Nubia sandstones. The average bulk magnetic susceptibility increased from 5.56×10^{-5} to 10.44×10^{-2} SI units, which in turns led to more consistent and reliable anisotropy data. Unexpectedly, an absolute angle $>60^{\circ}$ is observed between the declination of χ_1-pore and χ_1-grain for half of the samples, whereas the others have angles in the range 30–60°, with the exception of two sites still have nearly the same directions for the pore and grain maximum susceptibility, Ad 3 and Ks 3 (Fig. 18). This gave rise to one question: do the grain and pore lineations have different origins?

However, it seems that the grain fabric originates mainly from palaeocurrents flowing in the NE–SW and NNE–SSW directions, whereas the pore fabric seems to be controlled by later groundwater flow in a direction roughly perpendicular from the palaeocurrents responsible for the deposition. These palaeoflows are thought to be responsible for rebuilding the original pore space network into the present directions. This later groundwater migration was responsible for dissolution and reprecipitation of the oolitic ironstone into the vertical joints and fractures. These dominant joints are thought to postdate the deposition of Abu Ballas and Sabayia formations which are separated from the underlying Abu Simbil and the overlying Kesieba Formation by two main faulting processes.

These deposits were studied by many authors, for example, Haase (1993), Germann *et al.* (1987), Fischer (1989) and Mücke (2000), etc. They assigned an age of upper Cretaceous (Coniacian–Santonian), prior to the deposition of Kesieba Formation.

Mücke (2000) proposed that ferruginization is the consequence of descending meteoric waters that caused dissolution, migration and precipitation of various elements depending on the prevailing Eh/pH conditions. Ferruginization advanced through the permeable rock in a roll front-like manner completely or partially affecting the deposit from the top to the base. The pH of these solutions were suitable to attack and dissolve the outer rims of the quartz grains giving rise to skeletons of quartz and therefore were able to deviate the original direction of the pore network. The recharge areas of these meteoric waters are thought to be in the SSW of Tushka area and then flowed following the main relief of Sabayia Formation to the N direction. Another cycle of flowing meteoric water is thought to postdate the deposition of Kesieba Formation and had the main trend of the first flowing cycle to the NNW.

Finally, we note that one site at the top of Adindan Formation and another one at the top of Kesieba Formation still retains the

Downloaded from https://academic.oup.com/gji/article/177/1/43/729241 by guest on 26 June 2022

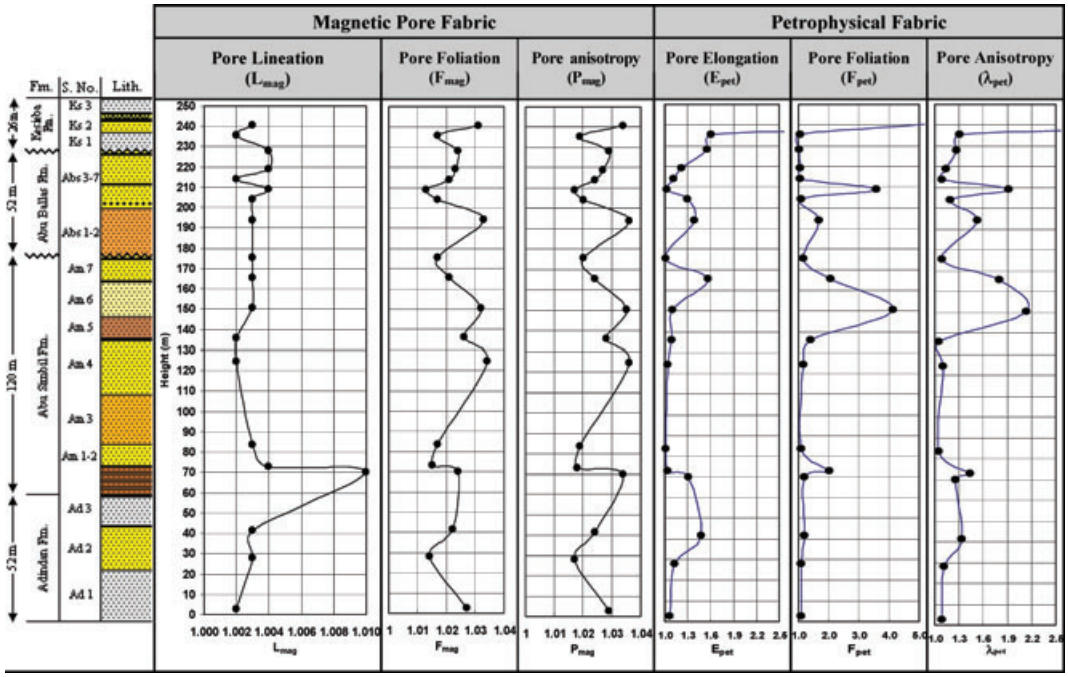

Figure 15. Vertical plot for the magnetic and petrophysical pore fabric parameters of the Nubia sandstones.

direction of the original depositional palaeocurrents. This could be explained by the fact that the invading diagenetic solutions failed to weaken, dissolve and to reorient the main trend of the grain skeleton of these sites and therefore failed to shift the original pore space net directions. Samples from these sites are characterized by relatively high hardness, less matrix dissolution and preservation of the quartz grains.

The imbrication angles for both the magnetic grain and pore fabrics and the AMS parameters, in general, indicate gentle slope bedding for the Nubia sandstone samples. From the field observations, the Nubia sandstones are mostly horizontally bedded except for Abu Ballas Formation which has gentle tilted-bedding; it has dip angle varies between 5° and 10°.

On the other side, the petrophysical pore fabric is characterized by very high porosity and permeability values exceeding the Levorsen's ranks (1967). So, it was better to extend this rank for the present highly porous and permeable sandstone as follows to cover the full range of the measured data.

Negligible :	$0 < \emptyset \leq 5$ per cent
Poor :	$5 < \emptyset \leq 10$ per cent
Fair :	$10 < \emptyset \leq 15$ per cent
Good :	$15 < \emptyset \leq 20$ per cent
Very good :	$20 < \emptyset \leq 25$ per cent
Excellent :	$25 < \emptyset$ (new rank)

(Modified after Levorsen 1967)

In addition, we tend to add another permeability rank more than 1000 mD described for excellent permeable rocks as follows.

Fair :	$1 < K \leq 10$ md
Good :	$10 < K \leq 100$ md
Very good :	$100 < K \leq 1000$ md
Excellent :	$1000 < K$ (new rank)

(Modified after Levorsen 1967)

Following the present modification, the measured porosity and permeability values indicate very good to excellent storage capacity properties for the Nubia sandstones.

Measuring permeability in three orthogonal directions led to a new concept called petrophysical pore fabric introduced in this study to better approach the pore shape in 3-D. It depends on the anisotropy of pore spaces, which in turn contributed by the pore elongation and foliation.

From this study and following the classification introduced by Nabawy and El-Hariri (2008) to classify the electric fabrics of some sandstone samples from Abu Gharadig basin in Egypt, we tend to introduce a new classification for the petrophysical pore fabric parameters (Table 4).

From this classification, the petrophysical pore fabric of the present sandstones are characterized by slight pore elongation, foliation and anisotropy for Adindan samples; slight pore elongation, moderate pore foliation and slight anisotropy for Abu Simbil and Abu Ballas samples; and moderate to high pore elongation, foliation and anisotropy for Kesieba samples. Some high to very high values have been detected for some samples, for example, Am 6, Abs 6 and Ks 3.

The cyclic behaviour of porosity and permeability between formations may be attributed to the fluvial depositional nature of the present rock. In addition, since, the Nubia sandstones are petrographically similar and devoid of macro and micro fauna, therefore, increasing the pore anisotropy at some levels could be attributed to some structural events rather than biological effects.

A comparison between Figs 11 and 15 indicates that increasing pore anisotropy is accompanied with decreasing measured permeability values, that is, the less the anisotropic pore shape, the higher the permeability values. Since the samples used for measuring permeability were cored in the main directions revealed from the magnetic pore studies, therefore it was expected to relate the anisotropy of both the magnetic and petrophysical pore fabrics as shown in Fig. 19. The magnetic pore foliation could also be related to the petrophysical pore foliation as shown in Fig. 20, whereas no

Downloaded from https://academic.oup.com/gji/article/177/1/43/729241 by guest on 26 June 2022

Table 3. Petrophysical permeability values of the studied Nubia sandstones measured in three orthogonal directions in the different directions.

Formation	S. no.	(K_V)	(K_{NE})	(K_{NW})	(K_b)	Rank	E_{pet}	F_{pet}	λ_{pet}	Direction of K_{max}
Kesieba formation										
	Ks 3	81.5	530.9	14.7	209.0	Very Good	6.51	5.54	6.01	
	Ks 2	2413.1	2564.9	4123.7	3033.9	Excellent	1.61	1.06	1.31	
	Ks 1	4800.2	4969.2	7750.0	5839.8	Excellent	1.56	1.04	1.27	
	Mean	2431.6	2688.3	3962.8	3027.6	Excellent	3.23	2.55	2.86	
Abu Ballas formation										
	Abs 7	155.2	203.6	166.4	175.1	Very Good	1.22	1.07	1.15	
	Abs 6	3322.4	2980.2	2783.2	3028.6	Excellent	1.11	1.07	1.09	
	Abs 5	324.0	1161.0	1198.2	894.4	Very Good	1.03	3.58	1.92	
	Abs 4	1632.5	1258.8	1135.6	1342.3	Excellent	1.30	1.11	1.20	
	Abs 3	7570.7	6830.2	6689.9	7030.3	Excellent	1.11	1.02	1.06	
	Abs 2	2154.0	5012.6	3628.4	3598.3	Excellent	1.38	1.68	1.53	
	Abs 1	4410.4	3736.3	4484.2	4210.3	Excellent	1.02	1.18	1.10	
	Mean	2795.6	3026.1	2869.4	2897.0	Excellent	1.17	1.53	1.29	
Abu Simbil formation										
	Am 7	529.4	1706.3	1090.2	1108.6	Excellent	1.57	2.06	1.80	
	Am 6	33.9	154.2	139.8	109.3	Very Good	1.10	4.12	2.13	
	Am 5	432.4	615.2	674.0	573.9	Very Good	1.56	0.70	1.05	
	Am 4	589.6	723.0	698.2	670.3	Very Good	1.04	1.18	1.11	
	Am 3	2694.8	2736.9	2476.6	2636.1	Excellent	1.02	1.09	1.05	
	Am 2	2990.2	2890.8	1432.7	2437.9	Excellent	1.03	2.02	1.44	
	Am 1	4406.4	7008.0	5334.6	5583.0	Excellent	1.31	1.21	1.26	
	Mean	1668.1	2262.1	1692.3	1874.2	Excellent	1.23	1.77	1.41	
Adindan formation										
	Ad 3	388.8	263.8	217.3	290.0	Very Good	1.47	1.21	1.34	
	Ad 2	1516.3	1653.4	1872.5	1680.7	Excellent	1.13	1.09	1.11	
	Ad 1	2285.7	2561.0	2732.2	2526.3	Excellent	1.07	1.12	1.09	
	Mean	1396.9	1492.7	1607.3	1499.0	Excellent	1.22	1.14	1.18	

Notes: K_V is the measured petrophysical permeability of the studied samples cored in a direction perpendicular to the bedding plane, K_{NE} for samples cored parallel to the bedding plane in the NE direction, K_{NW} for samples cored parallel to the bedding plane in the NW direction, and K_b is the average permeability. For the anisotropy parameters; E_{pet}, is the petrophysical pore elongation; F_{pet}, the pore foliation and λ_{pet}, is the petrophysical anisotropy of pore spaces.

Downloaded from https://academic.oup.com/gji/article/177/1/43/729241 by guest on 26 June 2022

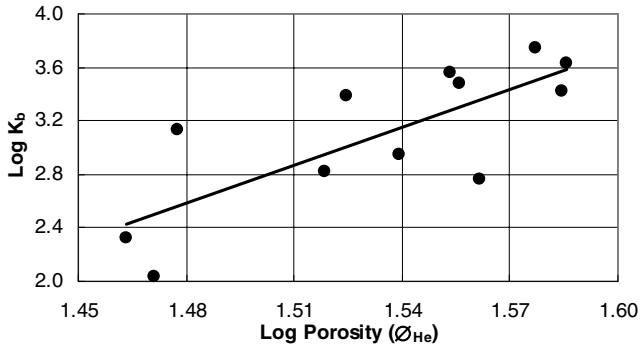

Figure 16. Plot of the measured bulk permeability (K_b) values against the porosity values measured by helium injection ($Ø_{He}$).

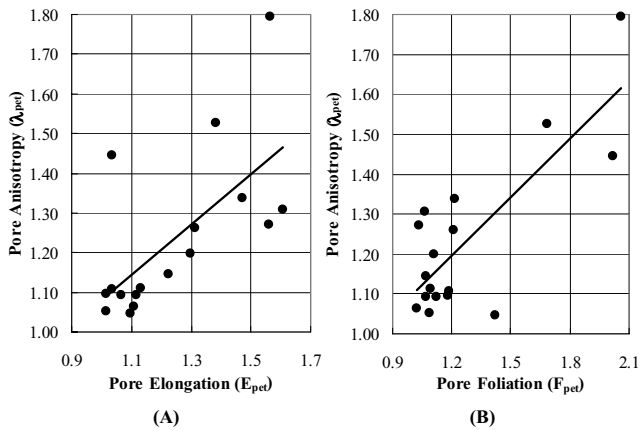

Figure 17. Dependence of the petrophysical pore anisotropy (λ_{pet}) on both: (A) Pore Elongation (E_{pet}) and (B) Pore Foliation (F_{pet}).

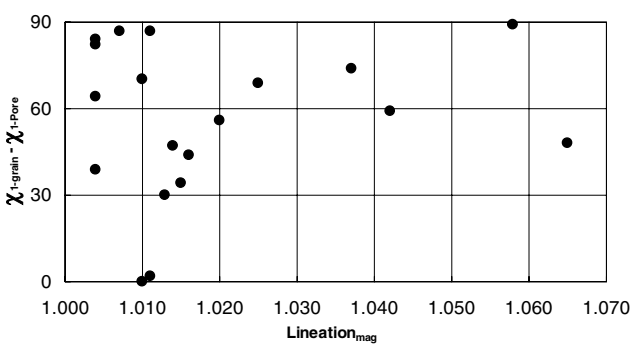

Figure 18. Plotting the absolute difference in declination's angle between magnetic grain and pore fabrics ($\chi_{1-\text{grain}} - \chi_{1-\text{pore}}$) versus the magnetic grain lineation (L_{mag}) for the studied sandstone samples.

relationship between the magnetic pore lineation and the petrophysical pore elongation was observed ($r = \pm 0.15$).

$$\lambda_{pet} = 3141 P_{mag}^2 - 6422 P_{mag} + 3284 \quad (r = \pm 0.58)$$

$$F_{pet} = 9674 F_{mag}^2 - 19734 F_{mag} + 10065 \quad (r = \pm 0.63).$$

This could be explained by that both the magnetic and petrophysical foliations are the main contributors to the anisotropy values for both the magnetic and petrophysical fabrics. Moreover, the petrophysical pore elongation is mainly raised from the maximum permeability values, which sometimes are in a vertical direction due to the presence of some vertical fracture porosity. These fractures seem to be of micro size and not accessible to the injected ferrofluid (injected at low pressure) which have relatively higher molecular size than that of the nitrogen molecules used for the permeability measurements at higher pressures.

Table 4. Classification of the petrophysical pore elongation, foliation, and anisotropy using the permeability values measured in three orthogonal directions.

Pore elongation (E_{pet})	Pore foliation (F_{pet})	Pore anisotropy (λ_{pet})
No elongation 1.0–1.1	No foliation 1.0–1.1	Isotropic 1.0–1.1
Slight 1.1–1.5	Slight 1.1–1.5	Slight 1.1–1.5
Moderate 1.5–2.5	Moderate 1.5–2.5	Moderate 1.5–2.5
High 2.5–5.0	High 2.5–5.0	High 2.5–5.0
Very high >5.0	Very high >5.0	Very high >5.0

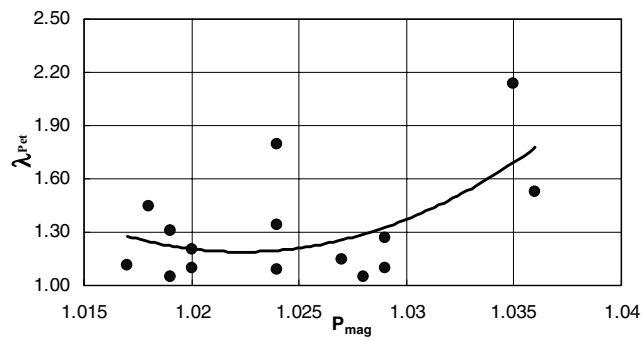

Figure 19. Plot of anisotropy of the petrophysical pore fabric (λ_{pet}) against the anisotropy of the magnetic pore fabric (P_{mag}).

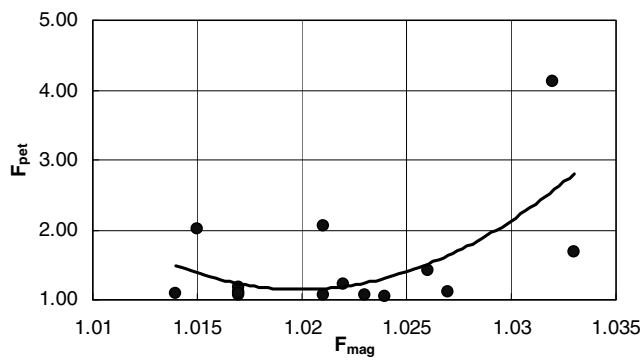

Figure 20. *X–Y* plot for the petrophysical pore foliation (F_{pet}) against the magnetic pore foliation (F_{mag}).

An overall coincidence between the petrophysical and magnetic pore fabrics is established. Petrophysical and magnetic pore fabrics of Adindan and Kesieba formations refer mostly to palaeocurrents flowed to the NNW direction, whereas refer to the NE for Abu Simbil samples. On the other side, pore fabrics of the Abu Ballas Formation seem to be structurally controlled, where the petrophysical pore fabric refers to pore elongation in the vertical direction as a main flow direction, whereas the magnetic pore fabrics refer to E–W direction.

The present flow directions have been proposed by Salem and Pallas (2001) who studied the sedimentological and hydrogeological system in the Nubia aquifer system and concluded that migration of the underground water is mainly directed to the NNW and NNE (Fig. 21). In addition, Kim *et al.* (2000) showed that, the groundwater in Tushka area between Lake Nasr and Darb El Arbein way (100–300 km, away from the Lake) flowing from SW to NE.

Downloaded from https://academic.oup.com/gji/article/177/1/43/729241 by guest on 26 June 2022

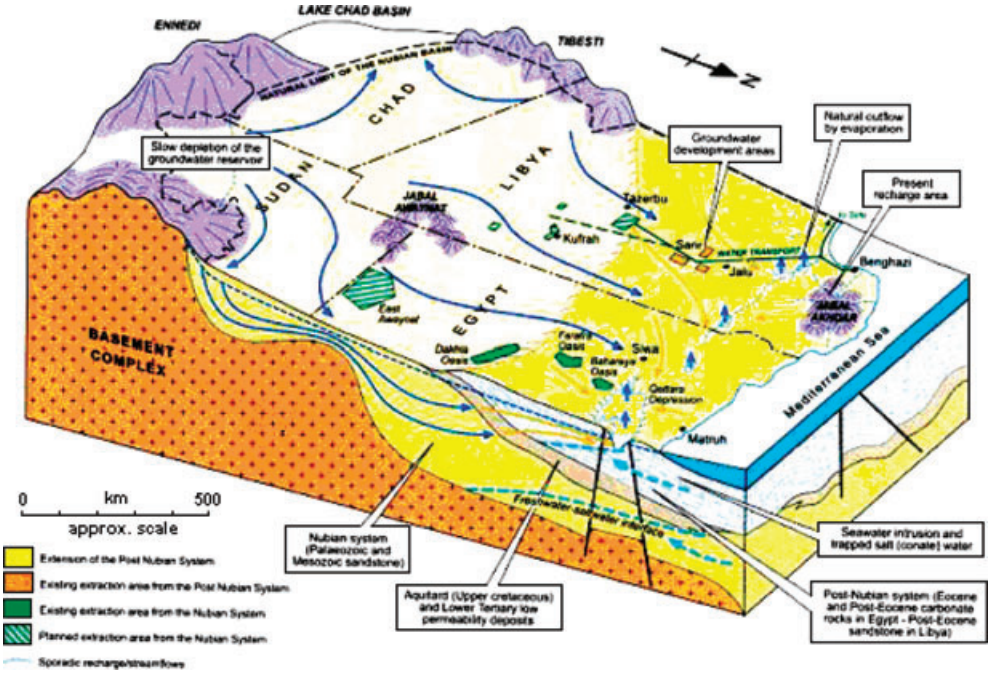

Figure 21. A 3-D schematic diagram of El Nuba area illustrating the hydrogeological system flowing mostly to the NNE and NNW directions (Salem & Pallas 2001).

Overall, the magnetic pore fabric method gives a reasonable estimate of the 3-D macrovoid anisotropy, but is considerably less effective in estimating the micro void anisotropy for which the permeability method is a better approach.

CONCLUSIONS

Petrographically, the Nubia sandstones in Tushka area are represented by quartz arenite composed of dissolved quartz grains cemented together by silica cement, which have suffered a long arid diagenetic history. Porosity of Nubia sandstones is very good to excellent. It varies between 20 and 35 per cent in the horizontal direction and between 15 and 25 per cent in the vertical direction indicating inhomogeneity in the distribution of the pore spaces.

Petrophysically, porosity values of the Nubia sandstones were measured by helium and ferrofluid injection. Values of ferrofluid porosity are always less than that of the helium porosity, due to the presence of some micro pore spaces could not be accessed by ferrofluid injection at low pressures.

The Nubia sandstones are characterized by very good to excellent permeability values which could be related to the helium porosity and weakly related to the ferrofluid porosity due to the presence of some micro pore spaces.

Anisotropy of pore spaces has been detected by measuring anisotropy of permeability (petrophysical pore fabric) and anisotropy of pore AMS in 3-D (magnetic pore fabric).

Magnetic pore data of Adindan and Kesieba formations refers to a pore elongation in the NNW–SSE direction, Abu Simbil Formation refers to the NE–SW, whereas directions of Ballas Formation follow the main fault trend in the study area, the E–W direction. The pore elongations are on average nearly perpendicular to the grain elongation directions.

The petrophysical pore fabric of the present sandstones have weak pore elongation, foliation and anisotropy for Adindan Formation and increases in intensity upwards into moderate to high pore elongation, foliation and anisotropy for Kesieba samples. The higher the permeability values, the lower the pore anisotropy values. The petrophysical pore fabric and both the magnetic fabrics are mainly planar.

The petrophysical pore fabrics of Adindan and Kesieba samples refer to pore spaces elongated in the NW–SE direction, and to the NE–SW direction for Abu Simbil samples, whereas the Abu Ballas samples mostly have maximum permeability in the vertical direction due to presence of some permeable fracture pore spaces.

In general, we find that the principal magnetic pore anisotropy directions coincide with the principal petrophysical pore anisotropy directions of the overall samples except for those from Abu Ballas Formation.

ACKNOWLEDGMENTS

We would like to thank Profs Philip Benson and Helga de Wall for their great comments that improved and reconstructed the manuscript. Thanks are also due to the Editor Prof Cor Langereis whose patience and insightful suggestions have led to a new concise revised version.

We are indebted to the Ministry of Foreign Affairs of France, the Ministry of Higher Education and State for Scientific Research of Egypt and the National Research Center (Egypt) for funding this work, under project code EGY/FR2–009, contract no. 17.

REFERENCES

Balsley, J.R. & Buddington, A.F., 1960. Magnetic susceptibility anisotropy and fabric of some Adirondack granites and orthogneisses, *Am. J. Sci.,* **258A,** 6–20.

Banerjee, S.K. & Stacey, F.D., 1967. The high field torque meter method of measuring magnetic anisotropy of rocks, in *Methods in Palaeomagnetism,* pp. 470–476, eds Collinson, D.W., Creer, K.M. & Runcorn, S.K., Elsevier, Amsterdam.

© 2009 The Authors, *GJI*, **177,** 43–61
Journal compilation © 2009 RAS

Downloaded from https://academic.oup.com/gji/article/177/1/43/729241 by guest on 26 June 2022

Benson, P.M., Meredith, P.G. & Platzman, E.S., 2003. Relating pore fabric geometry to acoustic and permeability anisotropy in Crab Orchard Sandstone: a laboratory study using magnetic ferrofluid, *Geophys. Res. Lett.,* **30**(19), 1976, doi:10.1029/2003GL017929.

Benson, P.M., 2004. Experimental study of void space, permeability and elastic anisotropy in crustal rock under ambient and hydrostatic pressure, *Ph.D. thesis*. University of London, London.

Benson, P.M., Meredith, P.G., Platzman, E.S. & White, R.E., 2005. Pore fabric shape anisotropy in porous sandstone and its relation to elastic and permeability anisotropy under isostatic pressure, *Int. J. Rock Mech.,* **42,** 890–899.

Crimes, T.P. & Oldershaw, M.A., 1967. Palaeocurrent determination by magnetic fabric measurements on the Cambrian rocks of St. Tudwal's Peninsula, North Wales, *Geol. J.,* **5,** 217–232.

Dickson, J.A.D., 1966. Carbonate identification and genesis revealed by staining, *J. Sed. Petrol.,* **36,** 491–505.

Du Bernard, X. & Carrio-Schaffhauser, E., 2003. Kaolinitic meniscus bridges as an indicator of early diagenesis in Nubian sandstones, Sinai, Egypt. *Sedimentology,* **50,** 1221–1229.

Durrast, H. & Siegsmund, S., 1999. Correlation between rock fabrics and physical properties of carbonate reservoir rocks, *Int. J. Earth Sci.,* **88,** 392–408.

EGPC-CONOCO, 1987. *Geological Map of Egypt,* NF 36 NW, El Saad El Ali, 1: 500, 000.

El-Sorady, A.I. & Abdallah, A.A., 2001. Geotechnical studies on the area of new Tushka city, *Ann. Geol. Surv. Egypt,* ***xxiv*,** 521–539.

Ellwood, B.B., Hrouda, F. & Wagner, J.J., 1988. Symposia on magnetic fabric; Introductory comments. *Phys. Earth planet. Inter.,* **51,** 249–252.

Fischer, K., 1989. Prozesse und Produkte lateritischer Verwitterung in oberkretazischen Sedimenten Oberägyptens und des Nordsudans, *Berl. Geowiss. Abh. (A),* **115,** 123.

Germann, K., Mücke, A., Doering, T. & Fischer, K., 1987. Late Cretaceous laterite-derived sedimentary deposits (oolitic ironstone, kaolins, bauxites) in Upper Egypt, *Berli. Geowiss. Abh. (A),* **75**(3), 727–758.

Granar, L., 1958. Magnetic measurements on Swedish varved sediments. *Arkiv Geofys.,* **3,** 1–40.

Haase, J., 1993. Vergleichende Untersuchungen yon eisenreichen oolithischen Kaolinit- und Bauxitvorkommen mit oolithischen Eisenerzen. Eine erzpetrographisch-mikroanalytische Untersuchung, *Ph.D. thesis*. Georg-August-Universitäit, Göttingen, Germany.

Hamilton, N. & Rees, A.I., 1970a. The use of magnetic fabric in palaeocurrent estimation, in *Palaeogeophysics,* pp. 445–464, ed. Runcorn, S.K., Academic press, London.

Hamilton, N. & Rees, A.I., 1970b. Magnetic fabric of sediments from the shelf La Jolla, California, *Marine Geol.,* **9/M,** 6–11.

Hendriks, F., 1988. Evolution of the depositional environments of SE Egypt during the Cretaceous and Lower tertiary, *Berli. Geowiss. Abh A,* **75**(1), 49–82.

Hermina, M., Klitzsch, E. & List, F.K., 1989. *Stratigraphic Lexicon and Explanatory notes to the Geological Map of Egypt, 1:500,000,* pp. 263, Conoco Inc., Cairo.

Hrouda, F., 1982. Magnetic anisotropy of rocks and its application in geology and geophysics, *Geophys. Surv.,* **5**(1), 37–82.

Hrouda, F., Hanak, J. & Terzijski, I., 2000. The magnetic and pore fabrics of extruded and pressed ceramic models, *Geophys. J. Int.,* **142,** 941–947.

Ising, G., 1942. On the magnetic properties of varved clay, *Ark. Mat. Astr. Phys.,* **29**(A), 1–37.

Issawi B., 1973. Nubia sandstone type section, *Bull AAPG,* **57**(4), 741– 745.

Issawi, B., 1978. Geology of the Nubia west area, western Desert, Egypt, *Ann. Geol. Surv. Egypt,* **viii,** 237–253.

Issawi, B. & Jux, U., 1982. Contribution to the stratigraphy of Paleozoic rocks in Egypt, *Geol. Surv. Egypt,* paper no. 64, 28.

Issawi, B. & Osman, R.A., 1993. Tectonic-Sedimentary synthesis of Paleozoic-Cretaceous clastics, SW Aswan, Egypt, *J. Sed. Soc. Egypt,* **1,** 11–22.

Jelinek, V., 1978. Statistical processing of anisotropy of magnetic susceptibility measured on groups of specimens, *Studia Geoph. Geod.,* **22,** 50–62.

Jelinek, V., 1981. Characterization of magnetic fabric of rocks. *Tectonophysics,* **79,** 563–567.

Jones, C. & Meredith, P.G., 1998. An experimental study of elastic wave propagation anisotropy and permeability anisotropy in an illitic shale, in Eurock '98, *Rock Mech. Petrol. Eng.,* **2,** 307–313.

Jones, S., Benson, P. & Meredith, P., 2006. Pore fabric anisotropy: testing the equivalent pore concept using magnetic measurements on synthetic voids of known geometry, *Geophys. J. Int.,* **66,** 485–492.

Ketzer, J.M., De Ros, L.F. & Dani, N. 2005. Kaolinitic meniscus bridges as an indicator of early diagenesis in Nubian sandstones, Sinai, Egypt—discussion, *Sedimentology,* **52,** 213–217.

Kim, J., Sultan, M., Criss, R., Salem, H. & Kassem, M.A., 2000. Hydrologic Impacts of the Tushka Canal: Inferences from groundwater modeling and stable isotopic compositions of surface and groundwater samples, *Eos Trans. AGU Meet., San Francisco*, **81**(48), Abst. xxxxx-xx.

Klitzsch, E., 1979. Zur Geologie des Gilf Kebir Gebietes in der Ost Sahara, *Clauth. Geo. Abh.,* **30,** 113–132.

Levorsen, A.I., 1967. *Geology of Petroleum,* W.H. Freeman Company, San Francisco, USA.

Lo, T.W., Coyner, K.B. & Toksoz, M.N., 1986. Experimental determination of elastic anisotropy of Berea sandstone, Chicopee shale, and Chelmsford granite, *Geophysics,* **51,** 164–171.

Louis, L., David, C., Metz, V., Robion, P., Menendez, B. & Kissel, C., 2005. Microstructural control on the anisotropy of elastic and transport properties in undeformed sandstones, *Int. J. Rock Mech.,* **42,** 911–923.

Mousa, M.F., 1984. Interpretation of magnetic anomalies of the Aswan-Tushka area, Western Desert, Egypt, *M.Sc. thesis*. Assuit Univ., Egypt.

Mücke, A, 2000. Environmental conditions in the Late Cretaceous African Tethys: conclusions from a microscopic-microchemical study of ooidal ironstones from Egypt, Sudan and Nigeria, *J. Afr. Earth Sci.,* **30**(1), 25–46.

Nabawy, B.S. & El-Hariri, T.Y., 2008. Electric fabric of subsurface Cretaceous rock, Abu Gharadig basin, Western Desert, Egypt, *J. Afr. Earth Sci.,* **52**(1–2), 55–61.

Nagata, T. 1961. *Rock Magnetism,* 350, Maruzen, Tokyo.

Noltimier, H.C., 1971. A model for grain dispersion and magnetic anisotropy in sedimentary rocks, *J. Geophys. Res.,* **76**(17), 3990–4000.

Pettijohn, F.J., 1984. *Sedimentary Rocks,* 3rd ed., CBS Publishers & Distributors, New Delhi.

Pfleiderer, S. & Halls, H.C., 1990. Magnetic susceptibility anisotropy of rocks saturated with ferrofluid, a new method to study pore fabric, *Phys. Earth planet. Inter.,* **65,** 158–164.

Pfleiderer, S. & Halls, H.C., 1993. Magnetic pore fabric analysis, verification through image autocorrelation, *J. geophys. Res.,* **98,** 4311–4316.

Pfleiderer, S. & Halls, H.C., 1994. Magnetic pore fabric analysis, a rapid method for estimating permeability anisotropy, *Geophys. J. Int.,* **116,** 39–45.

Pfleiderer, S. & Kissel, C., 1994. Variation of pore fabric across a fold-thrust structure. *Geophys. Res. Lett.,* **21**(19), 2147–2150.

Ragab, M.A., El Sayed, A.A. & Nabawy, B.S., 2000. Physical parameters of Egyptian oil reservoir sedimentary rocks: a review, in *Sedimentary Geology of Egypt: Applications and Economics,* pp. 129–150, ed. Soliman, S.M., Sedimentological society of Egypt, Cairo.

Rasolofosaon, P.N.J. & Zinszner, B.E., 2002. Comparison between permeability anisotropy and elastic anisotropy of reservoir rocks, *Geophysics,* **67,** 230–240.

Rathor, J.S., 1975. Studies of magnetic susceptibility anisotropy in rocks, *Ph.D. thesis*. New Castle Univ., England.

Rees, A.I., 1966. The effect of depositional slopes on the anisotropy of magnetic susceptibility of laboratory deposited sands, *J. Geol.,* **74,** 856–867.

Rees, A.I. & Woodball, W.A., 1975. The magnetic fabric of some laboratory deposited sediments, *Earth planet. Sci. Lett.,* **25,** 1221–1230.

Robinson, C.A., Werwer, A., El-Baz, F., El-Shazly, M., Fritch, T., & Kushy, T., 2007. The Nubian Aquifer in Southwest Egypt. *J. Hydrogeol.,* **15,** 33–45.

Rochette, P., 1987. Magnetic susceptibility of the rock matrix related to magnetic fabric studies, *J. Str. Geol.,* **9**(8), 1015–1020.

Downloaded from https://academic.oup.com/gji/article/177/1/43/729241 by guest on 26 June 2022

Rochette, P., Aubourg, C. & Aubourg, C., 1992. Rock magnetism and the interpretation of anisotropy of magnetic susceptibility, *Rev. Geophys.,* **30**(3), 209–226.

Said, R., 1962. *The Geology of Egypt,* pp. 218–287, Elsevier Pub. Co., Amsterdam.

Salem, O. & Pallas, P., 2001. The Nubian Sandstone Aquifer System (NSAS). in *International Shared (Transboundary) Aquifer Resources Management—Their Significance and Sustainable Management,* pp. 41–44, ed. Puri, S., IHP-VI, IHP Non Serial Publications in Hydrology, UNESCO, Paris.

Stacey, F.D., Joplin, G. & Lindsay, J., 1960. Magnetic anisotropy and fabric of some foliated rocks from S.E. Australia, *Geophys. Pure. Appl.,* **47,** 30–40.

Tarling, D.H. & Hrouda, F., 1993. *The Magnetic Anisotropy of Rocks,* 219, Chapman and Hall, London.

Thabit, G.K., 1994. Sedimentology of the Nubia group in the area southwest of Aswan, Abu Simbil area, *M.Sc. thesis*. Assuit Univ., Egypt.

Wood, D.S., Oertel, G., Singh, J. & Bennet, M.F., 1976. Strain and anisotropy in rocks, *Phil. Trans. R. Soc. Lond,* **283,** 27–42.

Downloaded from https://academic.oup.com/gji/article/177/1/43/729241 by guest on 26 June 2022